

Long-term IR Photometry of Seyferts

I.S. Glass

South African Astronomical Observatory, PO Box 9, Observatory 7935, South Africa

Received 2003

ABSTRACT

Long-term (up to 10000d) monitoring has been undertaken for 41 Seyferts in the near infrared (1.25 – 3.45 μ m). All but two showed variability, with amplitudes at K in the range < 0.1 to >1.1 mag. The timescale for detectable change is from about one week to a few years.

Where contemporary observations of variability in x-rays, UV or visible light exist, it is found that the near-infrared varies in a similar way, though in some cases the shorter-wavelength IR bands are diluted by underlying galaxy radiation.

A simple cross-correlation study indicates that there is evidence for delays of up to several hundred days between the variations seen at the shortest wavelengths (U or J) and the longest (L) in many galaxies. In particular, the data for Fairall 9 now extend to twice the interval covered in earlier publications and the delay between its UV and IR outputs is seen to persist.

An analysis of the fluxes shows that, for any given galaxy, the colours of the variable component of its nucleus are usually independent of the level of activity. The state of activity of the galaxy can be parameterized.

Taken over the whole sample, the colours of the variable components fall within moderately narrow ranges. In particular, the $H - K$ colour is appropriate to a black body of temperature 1600K. The $H - K$ excess for a heavily reddened nucleus can be determined and used to find E_{B-V} , which can be compared to the values found from the visible region broad line ratios.

Using flux-flux diagrams, the flux within the aperture from the underlying galaxies can often be determined without the need for model surface brightness profiles. In many galaxies it is apparent that there must be an additional constant contribution from warm dust.

Key words: galaxies: Seyfert – active – nuclei – photometry

1 INTRODUCTION

This programme was started with the aim of making a reliable study of the variability of Seyfert galaxies in the near infrared ($JHKL$ bands; 1.25, 1.65, 2.2 and 3.45 μ m). Previous work had indicated that some Seyfert galaxies do vary, but the data remained somewhat sparse and controversial. At the commencement of the programme it was believed, for example, that Seyfert 1 galaxies varied but Seyfert 2 galaxies did not. A 450-day programme by Penston et al (1974) appeared to confirm this viewpoint. Lebofsky & Rieke (1980) reported on variations observed in several Seyferts, of which that in 3C 120 was the most spectacular, but the numbers of observations were very limited.

Some results from this programme have already been published. One of the most unexpected was the discovery by Clavel, Wamsteker and Glass (1989) that there was a delay of 400 days between the UV variations of Fairall 9 and the

response of its infrared output. This was satisfactorily interpreted according to a dust reverberation model (Barvainis, 1987). NGC 1566 showed a delay of 2 ± 1 month between the UV and the IR (Baribaud et al, 1992). Similarly, a possible delay of ~ 85 d was seen in NGC 3783 (Glass, 1992). The infrared output of NGC 1068 was shown to have increased by a factor of two between the early 1970s and 1995 by Glass (1995). The galaxy NGC 2992 showed an energetic flare-like outburst with a decay time of about 900d (Glass, 1997a) and NGC 7469 showed a dramatic but relatively short-lived decline in its nuclear energy output in October 1989 (Glass 1998).

More recently, Salvati et al (1993) observed an outburst in NGC 4051 and Nelson (1996) reported one in Mkn 744, with a 32 ± 7 day delay between the visible and IR light curves. Oknyanskij & Horne (2001) have re-examined the published data and concluded that the observed delays are consistent with dust sublimation radii $R \propto \sqrt{L_{UV}}$. Oknyan-

skij (2002) includes two additional objects. The angular diameter of the dust ring or shell as viewed from the earth is of order tenths of milliarcsec.

Throughout this paper it is assumed that the excess infrared radiation from a Seyfert when compared to a less active galaxy comes from dust that is heated by ultraviolet radiation originating near a central massive black hole. It is usually assumed that this dust is distributed in a torus; e.g., Pier & Krolik (1992). The maximum temperature that dust can reach without sublimating, in the neighbourhood of 1600K, together with the ultraviolet luminosity of the nucleus, sets the inner radius of its distribution and the corresponding light travel time gives the delay in the response of a dust grain to a change in the ultraviolet flux from the nucleus.

During part of the present programme, *UBVRI* photometry was obtained by Winkler et al (1992), Winkler (1997) and other observers.

2 OBSERVATIONS

The choice of galaxies to observe was very simple: only a few southern Seyferts were known at the start of the programme. As others were discovered, by examination of the ESO and UK Schmidt plates or from x-ray satellites, they were included. The *L*-band luminosities (calculated from the redshifts and the fluxes seen through a 12 arcsec diameter aperture) range over three orders of magnitude. It will be seen later that the proportion of nuclear to underlying galaxy fluxes also covers a large range.

Nearly all the observations were made with the MkIII infrared photometer attached to the 1.9m telescope at Sutherland. The aperture was normally 12 arcsec diameter. In some cases, *L* observations were made at 9 arcsec diameter to improve the signal-to-noise ratio at slight expense to the systematic accuracy. The chopper throw was 30 arcsec, alternately north and south of the object position. The same filters were used throughout the programme.

Some of the earliest observations were made with the MkI infrared photometer, which used the same filters but had chopper throws of 12 or 60 arcsec, also in the N-S direction.

Standard stars were taken from Carter (1990), whose *J* measures were transformed to the natural system of the photometer using the empirical relation $J_{\text{natural}} = J_{\text{Carter}} - 0.05(J - H)_{\text{Carter}}$. The other bands were taken to be the same on both systems. The results were placed on the Carter system using the inverse transformation.

Table 1 lists the galaxies included in the survey. The positions, redshifts, Seyfert types, *l*, and *b* were taken from Véron-Cetty & Véron (2000). The absorption E_{B-V} arising in our own galaxy was calculated from the NASA/IPAC Database Extinction Calculator on the Worldwide Web, which is based on Schlegel, Finkbeiner & Davis (1998). The columns ΔJ and ΔK are the overall observed amplitudes observed at *J* and *K*, respectively. It should be noted that these two quantities are sensitive to errors in individual measurements, and are, in effect, upper limits. The column 'No' gives the number of observations of each object. The last three columns give the average dereddened near-IR colours.

Observations were usually made four times per year over

periods of a week. Usually a given galaxy could be observed three times per year, with one or two repeats within a few days. In a few cases, several observations were made over a short period as part of international multi-wavelength campaigns.

Figs 2 a,b,c,d show the observations plotted against time. The same time and magnitude scales are employed throughout, for ease of comparison. Additional data obtained by other workers in the *U* band have been included in several cases. The error bars have been plotted only when they are expected to be substantial. Normally, the standard errors at *JHK*, arising from the standard stars and the uncertainties in the extinctions, are expected to be $\lesssim 0.03$ mag and, at *L*, $\lesssim 0.05$ mag. In general, these are the dominant errors. However, at *L* the signal-to-noise ratio was reduced and observations were usually limited to about 320 sec of integration, so that the final errors may be higher than 0.05 mag, especially when $L > 9$.

The observations are available at the end of this version of the paper.

3 AVERAGE NEAR-IR COLOURS

The average, unweighted, de-reddened colours of the galaxies in the sample are given in the right-most columns of Table 1. De-reddening was carried out according to the relations

$$E_{B-V} : AJ : AH : AK : AL :: 1 : 0.742 : 0.430 : 0.245 : 0.094$$

The *J - H* and *H - K* colours of 'inactive', or early-type galaxies without obvious emission lines, on the same photometric system as that used here, are typically around 0.78 and 0.22 (Glass, 1984). The *K - L* colour (in the absence of dust emission) has been taken to be 0.22, based on the similarity of *H - K* and *K - L* colours for late-type stars (Glass, 1997c)

A few of the sample, NGC 1566, MCG-5-13-17, NGC 2110, I Zw 96, NGC 4748, NGC 6814 and NGC 7213, show *J - H* and *H - K* colours only moderately redder than inactive galaxies. This can also be seen in the vertical spacing of their light curves in Fig 2. When quiescent, the *L* light curve of a galaxy such as NGC 1566 is so close to the *K* curve that there is obviously no *L* excess. NGC 4748 and NGC 6814 also revert to inactive colours during minima. Their nuclear fluxes are assumed to be swamped by the stellar fluxes of the underlying galaxies at *J* and *H*, but may become more conspicuous at longer wavelengths because their spectral energy distributions rise and overcome the Rayleigh-Jeans tails of the stellar fluxes.

K - L excesses are seen at all times in MCG-5-13-17, NGC 2110 and NGC 7213, indicating continuous nuclear activity. NGC 7213 has positive *U - B*, indicating that its nucleus is heavily reddened.

On the other hand, in the case of ESO 103-G35, the *L* and *K* light curves are far apart, implying a considerable excess in spite of a lack of variability. Since its *H - K* colour is normal, the *L* excess must arise from a blackbody of about 800K or less. A positive *U - B* implies that its nucleus may be heavily reddened.

Most of the remainder of the sample show well-developed infrared excesses.

Table 1. List of galaxies in survey

Name	R.A. ¹ (2000)	Dec.	z^1	type ¹	$L_{3.4\mu\text{m}}$	E_{B-V}	ΔJ	ΔK	No.	$J-H$	$H-K$	$K-L$
III Zwicky 2	00 10 31.0	+10 58 28	.090	S1.2	23.72	.082	.66	.68	17	0.91	1.09	1.45
Tol 0109-38	01 11 27.7	-38 05 01	.011	S1.9	22.88	.014	.21	.34	31	1.27	1.14	1.76
F9	01 23 45.8	-58 48 21	.045	S1.2	23.66	.020	.78	1.15	71	1.00	0.91	1.45
NGC526A	01 23 54.4	-35 03 56	.019	S1.9	22.69	.022	.26	1.01	52	0.96	0.74	1.31
NGC985	02 34 37.8	-08 47 15	.043	S1.5	23.18	.030	.31	.48	7	0.89	0.66	1.13
ESO 198-G24	02 38 19.7	-52 11 32	.045	S1.0	23.10	.033	.62	.92	18	0.90	0.74	1.23
NGC1068	02 42 40.7	-00 00 47	.003	S1h	22.88	.030	.12	.60	27	1.01	1.03	2.16
NGC1566	04 20 00.7	-54 56 17	.004	S1.5	21.37	.008	.14	.28	42	0.83	0.29	0.42
3C120	04 33 11.1	+05 21 15	.033	S1.5	23.31	.297	.50	.53	30	0.93	0.90	1.41
Akn 120	05 16 11.4	-00 09 00	.033	S1.0	23.44	.109	.40	.52	32	0.96	0.82	1.28
MCG-5-13-17 ²	05 19 35.6	-32 39 30	.013	S1.5	22.12	.017	.15	.23	25	0.77	0.36	0.70
Pic A ³	05 19 44.3	-45 46 50	.034	S1.5	-	.043	.42	.33	14	1.00	0.96	
NGC2110	05 52 11.4	-07 27 23	.020	S1i	22.99	.375	.09	.10	15	0.85	0.34	0.69
H0557-383	05 58 02.1	-38 20 05	.034	S1.2	23.61	.046	.35	.37	33	1.14	1.11	1.78
F265	06 56 17.3	-65 33 48	.029	S1.2	22.74	.082	.20	.22	12	0.87	0.65	1.07
IRAS09149-6206	09 16 09.5	-62 19 29	.057	S1	24.32	.182	.24	.26	7	1.08	1.09	1.52
NGC2992	09 45 42.0	-14 19 35	.008	S1.9	22.17	.060	.38	.65	52	0.98	0.52	0.84
MCG-5-23-16 ⁴	09 47 40.2	-30 56 54	.008	S1.9	22.16	.108	.19	.37	25	0.86	0.51	1.17
NGC3783	11 39 01.8	-37 44 19	.009	S1.5	22.44	.119	.63	.90	95	0.86	0.72	1.31
H1143-182 ⁵	11 45 40.6	-18 27 17	.033	S1.5	22.77	.039	.70	.66	14	0.85	0.70	1.09
I Zwicky 96	12 00 43.3	-20 50 01	.062	S1	-	.051	.18	.19	13	0.78	0.44	
NGC4593	12 39 39.4	-05 20 39	.009	S1.0	22.26	.025	.17	.40	41	0.88	0.52	0.94
NGC4748 ⁶	12 53 12.4	-13 24 53	.014	S1n	21.95	.050	.16	.28	14	0.79	0.38	0.43
ESO 323-G77	13 06 26.6	-40 24 42	.015	S1.2	23.12	.101	.31	.49	27	1.09	0.84	1.22
MCG-6-30-15	13 35 53.4	-34 17 48	.008	S1.5	22.21	.062	.18	.18	25	0.88	0.66	1.25
IC4329A	13 49 19.3	-30 18 34	.016	S1.2	23.22	.059	.29	.46	38	0.97	0.87	1.48
NGC5506	14 13 14.8	-03 12 26	.007	S1i	22.71	.060	.37	.70	43	1.50	1.27	1.59
NGC5548	14 17 59.6	+25 08 13	.017	S1.5	22.81	.020	.22	.19	12	0.86	0.72	1.29
IRAS15091-2107	15 11 59.8	-21 19 02	.044	S1n	23.36	.118	.26	.27	10	0.92	0.82	1.33
ESO 103-G35	18 38 20.3	-65 25 42	.013	S1.9	22.20	.076	.16	.09	25	0.81	0.37	1.32
F51	18 44 54.0	-62 21 53	.014	S1.5	22.65	.108	.29	.37	29	1.00	0.84	1.34
ESO 141-G55	19 21 14.3	-58 40 13	.037	S1.2	23.36	.111	.59	.71	34	0.94	0.89	1.35
NGC6814	19 42 40.7	-10 19 24	.006	S1.5	21.50	.183	.19	.32	24	0.83	0.29	0.40
Mkn 509	20 44 09.7	-10 43 24	.035	S1.5	23.43	.057	.65	.62	46	0.91	0.88	1.35
1H2107-097	21 09 09.8	-09 40 17	.027	S1.2	23.00	.233	.26	.33	7	0.90	0.79	1.29
1H2129-624	21 36 23.2	-62 24 00	.059	S1.5	23.33	.037	.49	.72	6	0.94	0.80	1.31
NGC7213	22 09 16.4	-47 10 01	.006	S3b	22.14	.015	.12	.18	26	0.81	0.36	0.68
NGC7469	23 03 15.6	+08 52 26	.017	S1.5	23.05	.069	.31	.63	32	0.96	0.67	1.12
MCG-2-58-22	23 04 43.5	-08 41 08	.048	S1.5	23.44	.042	.87	1.17	49	0.94	0.80	1.31
NGC7603	23 18 56.7	+00 14 38	.029	S1.5	23.09	.046	.40	.87	26	0.89	0.59	1.05

Notes: Positions, redshifts and Seyfert types taken from Véron-Cetty & Véron (2000). Pic A and NGC 7213 have broad Balmer lines, but also exceptionally strong [OII] and many other typical liner characteristics. In the blue, NGC 2110 looks like a type 2, but near H α it has the spectrum of a liner (Winkler, private communication).

The E_{B-V} values are taken from the NASA/IPAC Database Extinction Calculator on the World Wide Web, which is based on Schlegel et al (1998).

The average luminosity at L , seen through the 12 arcsec diameter aperture, is given in units of $\log \text{WHz}^{-1}$ in the column marked $L_{3.4\mu\text{m}}$, taking H_0 as $65 \text{ km s}^{-1}\text{pc}^{-1}$.

ΔJ , ΔK are maximum amplitude ranges observed.

$J - H$ etc are the unweighted averaged de-reddened colours.

¹These columns are from Véron-Cetty & Véron (2000).

²Given by Véron-Cetty & Véron (2000) as ESO362-G18

³Given by Véron-Cetty & Véron (2000) as PKS0518-45.

⁴Given by Véron-Cetty & Véron (2000) as ESO434-G40.

⁵Given by Véron-Cetty & Véron (2000) as NPM1G-18.0386.

⁶Better known as IRAS1249-131

4 VARIABILITY PATTERNS

The galaxies of the sample do not show variability on a night-to-night basis, within the limits of the photometry. The only ones which may not have varied at all are NGC 2110 and ESO 103-G35. Most show smooth behaviour on a timescale of years, but some show shorter-term fluctuations. The most conspicuous of the latter is NGC 3783. An

active galaxy is thus more likely to be revealed by IR variability than by broad emission lines, which may be hidden from view by extinction within the host galaxy.

As already mentioned, two very interesting cases of large amplitude short-term events are seen in NGC 2992, which seems to have experienced a substantial outburst (Glass, 1997a) and NGC 7469, whose nuclear source virtually shut off for a short period (Glass, 1998).

Some galaxies show major changes over the long term. For example, the archetype S2 galaxy NGC 1068 doubled in L flux over about 20 years. NGC 4748 has become fainter over 2000d and ESO 323-G77 over 5000d. MCG-2-58-22 has declined by over a magnitude in 5000d, though not monotonically.

Otherwise, major variations, of more than one mag, have been seen in Fairall 9 and NGC 526a. Fairall 9 shows a delay between its UV output and its L flux, which can be detected even between the J and L bands. This has been satisfactorily explained in terms of dust-reprocessing by Clavel, Wamsteker & Glass (1989), using a model put forward by Barvainis (1987). The delay continues to exist in data obtained since the completion of the earlier work.

In many cases, the variability is most apparent at the longer wavelengths, especially L . This can have two causes, swamping at short wavelengths by the underlying galaxy in the 12 arcsec diameter aperture (as mentioned) and circumnuclear reddening, which is almost certainly present in NGC 1068.

Some constraint on the size of the emitting regions can be obtained from the timescale on which substantial variations can occur. If a dust re-emission model is accepted, the material may be distributed at different distances from the nucleus of the active galaxy and at arbitrary angles. Thus, the infrared response to an instantaneous change in the ultraviolet [e.g., $F_{\nu\text{uv}}(t) \propto \delta(t)$] will usually be smeared out. Only in the case of a ring of dust perpendicular to the line of sight can a very sharp response be expected (Barvainis, 1992).

5 SEARCH FOR DELAYS

A number of the galaxies in the present paper have been monitored at shorter wavelengths for various lengths of time and some of this work is included in Fig 2. The variations in U tend to have higher amplitude and possibly shorter time scales than those at infrared wavelengths.

Delays between the short-wavelength light curve(s), thought to be indicative of the UV flux from the central engine, and the L flux originating in the dust that it is heating, have been looked for using a simple cross-correlation programme based on the interpolation method of Gaskell & Peterson (1987). It should be emphasized that there are many opinions as to the best method for finding delays in cases where the data are irregularly spaced. A more detailed analysis will be carried out in a future paper.

The Gaskell & Peterson method was applied to those galaxies with significant variability and many data points. Ideally, the data should have been sampled at regular intervals, shorter than the expected delay times, for this procedure to be reliable. The programme first interpolates the longest wavelength photometry to give values for each day as well as extrapolating its starting and stopping values as constants for 1000 days before and after the series. Each light curve is shifted by a constant to have average value 0 and divided so as to have rms deviation 1. The cross-correlation is performed for the dates of the shorter-wavelength observations, using a range of 1000 days in each direction. The correlogram is divided by its maximum value so that the maximum of the peak is 1.0. Some of the causes that may

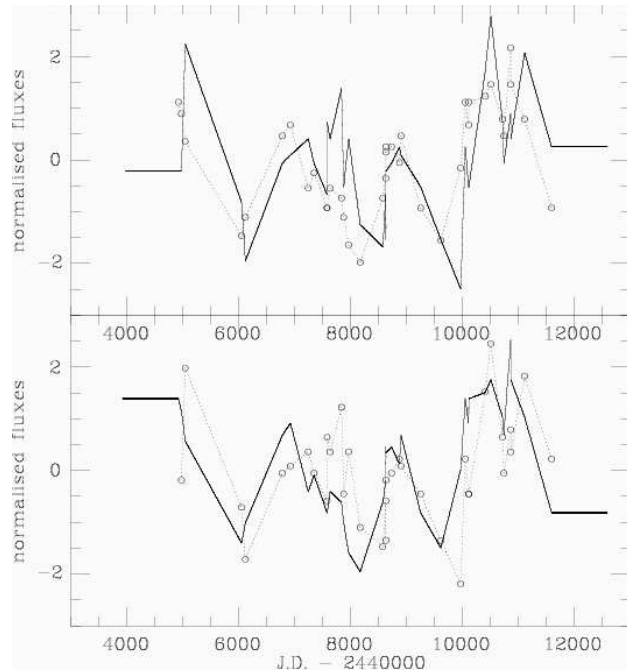


Figure 1. Data for H0557-383 adjusted to have mean value 0 and rms deviation 1, before cross-correlation. In the lower panel, the J data are interpolated and extrapolated and in the upper the L data are so treated. The interpolated data are given as solid lines and the non-interpolated data are joined with dotted lines.

distort the correlogram are (a) insufficient sampling (b) long gaps in the data, particularly if these coincide with enhanced activity (deviation from flat behaviour) (c) closely-clustered measurements, which cause over-weighting of certain sections of the non-interpolated sequences (d) an amplitude of variation that is not much greater than the noise, such as occurs at the J wavelength in some galaxies (e) noise (f) correlated errors from sampling of the two wavelengths quasi-simultaneously and (f) extrapolation of the data before and after the series, as described. No attempt was made to correct the data for these effects, except that some early and very sparsely sampled data were removed in a few cases. Allowances for these problems will be made in future analysis work, when possible.

The procedure is carried out twice, exchanging the two data sets, so that in the second case the shorter-wavelength data are interpolated instead of the longer. The position of the peak is taken to be the centre of the correlogram measured at the vertical level of 0.8 to avoid sometimes spiky peaks. The results are presented in Table 2. The technique used is known to be lacking in mathematical rigour, and can only be justified by the fact that almost all galaxies tried show some degree of delay between the U or J and the L light curves. To check the input data the shifted and divided data sets were plotted for inspection. In some cases the delay is obvious to the eye; fig 1 is an example of such a plot, for H0557-383. The L vs J cross-correlation gives 310d and the J vs L gives -300d. Averaging these two implies a delay of about 305d. The longer delays are likely to be the most certain and the shorter ones should be regarded as indicative only. If the cross-correlation has multiple peaks at the 0.8 level or greater it is rejected. In the case of MCG-

2-58-22 the J autocorrelation function was very broad, as were the cross-correlation peaks, although suggestive of a delay of several hundred days.

There is no guarantee that the delay between the ultraviolet and the infrared response is a constant quantity. The evaporation of dusty clouds near an AGN has been considered by Pier & Voit (1995) and it is clear that a prolonged period of high activity will cause the inner edge of the dust torus to retreat, increasing the propagation time for the UV radiation. According to Barvainis (1992), for an equilibrium situation, the radius within which particles will evaporate is

$$R_{\text{evap}} = 1.1 L_{46}^{0.5} e^{-\tau_{\text{UV}}/2} (T/1500\text{K})^{-2.8} (a/0.05\mu\text{m})^{-0.5} \text{pc},$$

where L_{46} is the UV luminosity in units of 10^{46}ergs^{-1} , τ_{UV} is the UV optical depth of the cloud, T is the temperature of the hottest grains and a is the grain radius in μm .

The present data show that long-term secular variations in the average infrared luminosity of Seyfert galaxies are quite common. Their UV luminosity is probably also variable, so that the Barvainis (1992) relation given above should be applied with caution if at all.

A possibility for further work, pointed out by Dr V.L. Oknyanskij (private communication), would be to concentrate on the K -band emission, which is likely to be more representative of the hottest dust component and may show a more precise response to ultraviolet variations than L .

6 SPECTRAL ENERGY DISTRIBUTIONS OF THE VARIABLE COMPONENTS

In the $UBVRI$ spectral region Winkler et al (1992) (see also Winkler, 1997) found that the fluxes from many Seyferts, when plotted against each other on linear scales, follow clear linear relationships. This effect had been observed previously by Choloniewski (1981) in NGC 4151 and a number of other active galaxies, QSOs and BL Lac objects. The implication is that the spectral energy distribution of the variable component is constant with time in a given galaxy and does not change with the level of activity. The slopes obtained from the linear flux-flux diagrams can be expressed as colours and it is found that they have some tendency to have values that are independent of the galaxy being considered. Galaxies with nuclei that are clearly perceived to be obscured have redder variable components.

The colours of the variable components have also been found to stay constant or very nearly constant in the near-infrared (Glass, 1992), and a number of examples have already been published: NGC 3783 (Glass 1992), NGC 1068 (Glass 1995), NGC 2992 (Glass 1997a) and NGC 7469 (Glass 1998). Figs 4a-f, 5 and 6 give data in the form of flux-flux plots for many of the galaxies in this paper. The linear relations between most pairs of colours are obvious. Only in the cases of III Zw 2, NGC2992, MCG-2-58-22 and NGC7603 do there seem to be changes of slope with intensity, in the L vs K diagram. These may be associated with long-term monotonic changes and are discussed in more detail below.

The infrared colours of the variable components of all the galaxies in this sample have been determined from the flux-flux plots. Each galaxy was first dereddened according to the E_{B-V} values given in Table 1 and the magnitudes were converted to fluxes using the calibration for a zeroth

Table 2. Delays between U or J and L , determined by the cross-correlation programme

Name	bands	delay (days)	bands	delay (days)	average ¹ (days)
III Zwicky 2	-				
Tol 0109-38	L, J	+100	J, L	-90	95
F9	L, U	+500	U, L	-440	470
F9	L, J	+370	J, L	-370	370
NGC526A	L, J	+120	J, L	-250	185
NGC985	-				
ESO 198-G24	-				
NGC1068	-				
NGC1566	-				
3C120	L, J	+160	J, L	-160	160
Akn 120	L, J	+120	J, L	0	60
Akn 120	L, U	+250	U, L	-380	315
MCG-5-13-17	-				
Pic A	-				
NGC2110	-				
H0557-383	L, J	+310	J, L	-300	305
F265	-				
IRAS09149-6206	-				
NGC2992	L, J	0	J, L	-70	35
MCG-5-23-16	-				
NGC3783	L, J	185	J, L	-110	148
NGC3783	L, U	200	U, L	-170	185
H1143-182	-				
I Zwicky 96	-				
NGC4593	L, J	110	J, L	0	55
NGC4748	-				
ESO 323-G77	-				
MCG-6-30-15	L, J	47	J, L	-20	34
IC4329A	L, J^2	135	J, L	70	33
IC4329A	L, J^2	150	J, L	-20	85
NGC5506	L, J	-10	J, L	-50 ³	25
NGC5548	-				
IRAS15091-2107	-				
ESO 103-G35	-				
F51	L, J	20	J, L	-10	15
ESO 141-G55	L, U	180	U, L	-280	230
ESO 141-G55	L, J	210	J, L	-100	155
NGC6814	L, J	80	J, L	0	40
Mkn 509	-				
1H2107-097	-				
1H2129-624	-				
NGC7213	-				
NGC7469	L, U	30	U, L	-12	21
NGC7469	L, J	110	J, L	+30	40
MCG-2-58-22	L, J	270	J, L	-500	155
NGC7603	-				

Notes:

¹ The ‘average’ column gives the average of the two ‘delay’ columns, for a delay in the sense long wavelength - short wavelength.

² The CCFs are asymmetric. At the usual level of 0.8 the delay is 33 d and at 0.7 it is 85 d.

³ The J vs L CCF is asymmetric. The delay is ~ 0 at the peak.

mag star of $\log(\text{flux}) = -22.82, -23.01, -23.21$ and $-23.55 \text{ Wm}^{-2}\text{Hz}^{-1}$ for J, H, K and L respectively. The procedure of Simon and Drake (1989), which assumes that all the scatter is due to observational error, was then used to calculate the regression coefficients F_{HJ} , F_{KH} and F_{LK} and their standard errors. The programme assumes constant JHK errors of 0.03 mag and L errors of 0.06 mag, which were exceeded in some cases.

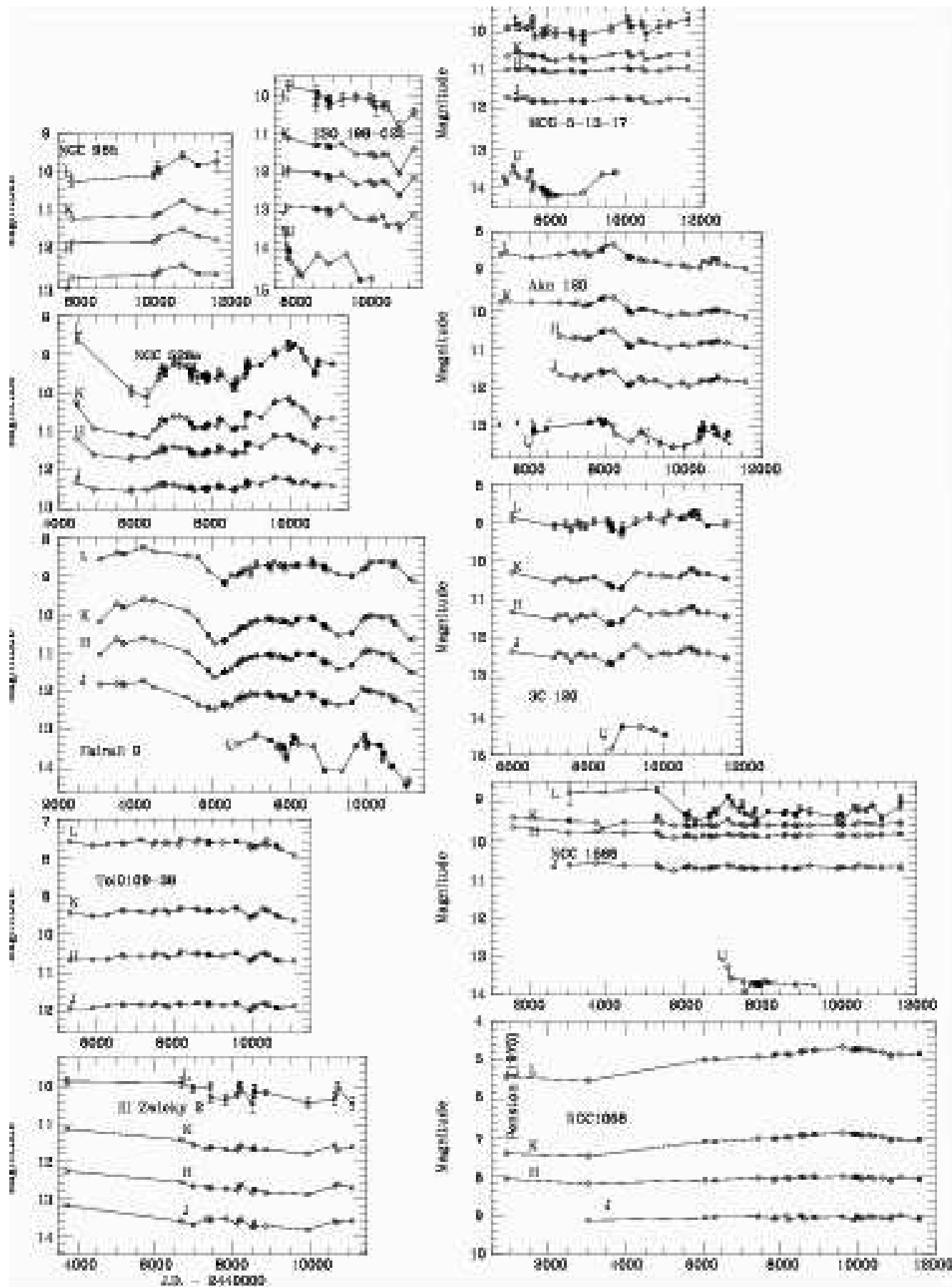


Figure 2. (a) *JHK_L* light curves for Seyfert galaxies, plotted on uniform magnitude and time scales.

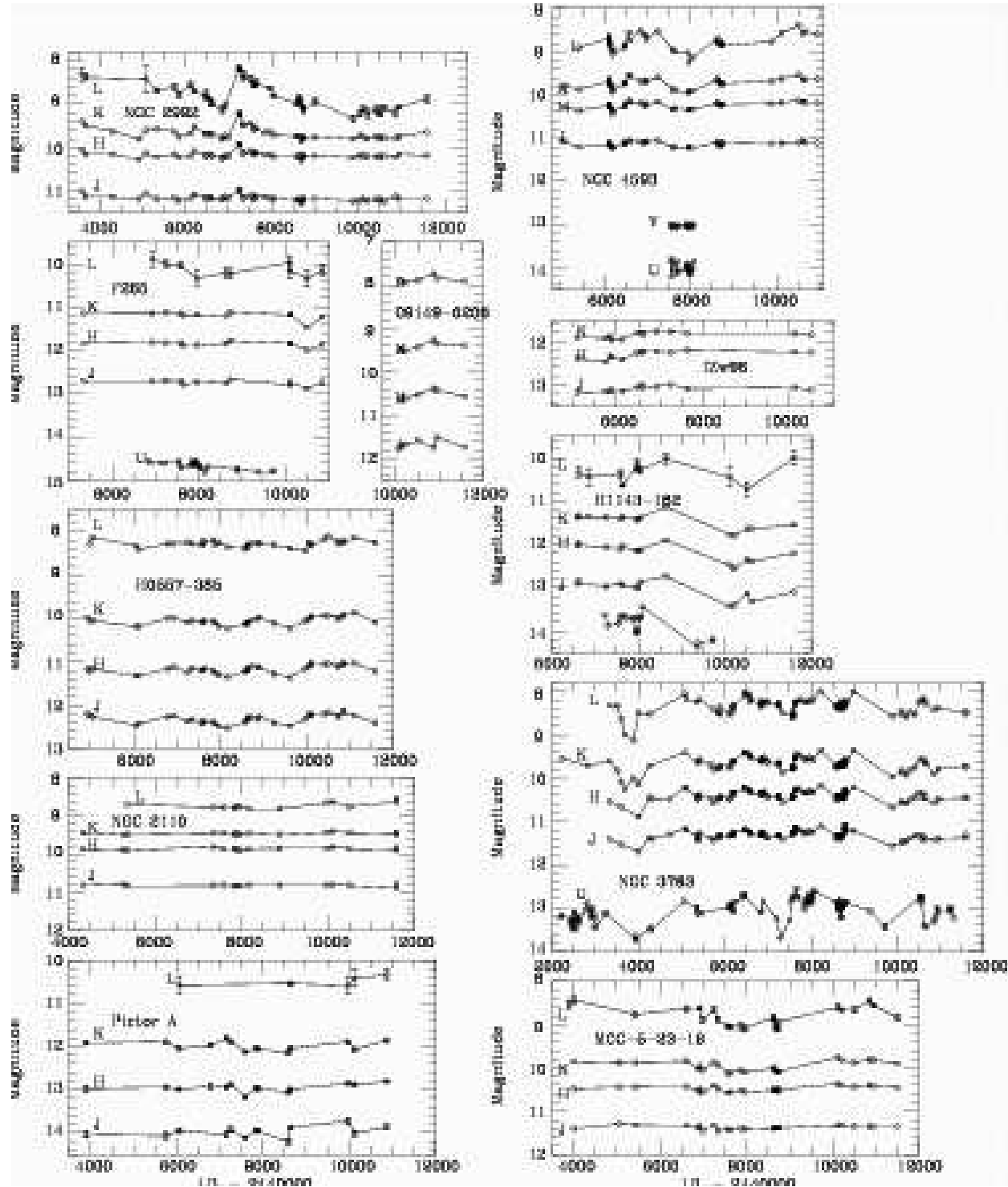


Figure 2. (b) Light curves for Seyfert galaxies

The colours of the variable components were calculated using the following formulae:

$$J - H = 2.5(\log F_{HJ} + 0.19)$$

$$H - K = 2.5(\log F_{KH} + 0.20)$$

$$K - L = 2.5(\log F_{LK} + 0.34).$$

The colours and errors are given in Table 3. The errors

can sometimes be quite large. They arise from (a) the variations in many cases being quite small (b) lower-quality photometry in the *L*-band, where the objects were often rather faint and (c) from uncertainties in the telluric extinction corrections at *L* and to a lesser extent at *J*. (The *H* and *K* extinctions of the earth's atmosphere track each other very well, so that the *H* - *K* colour is the most reliable; Glass & Carter, 1989).

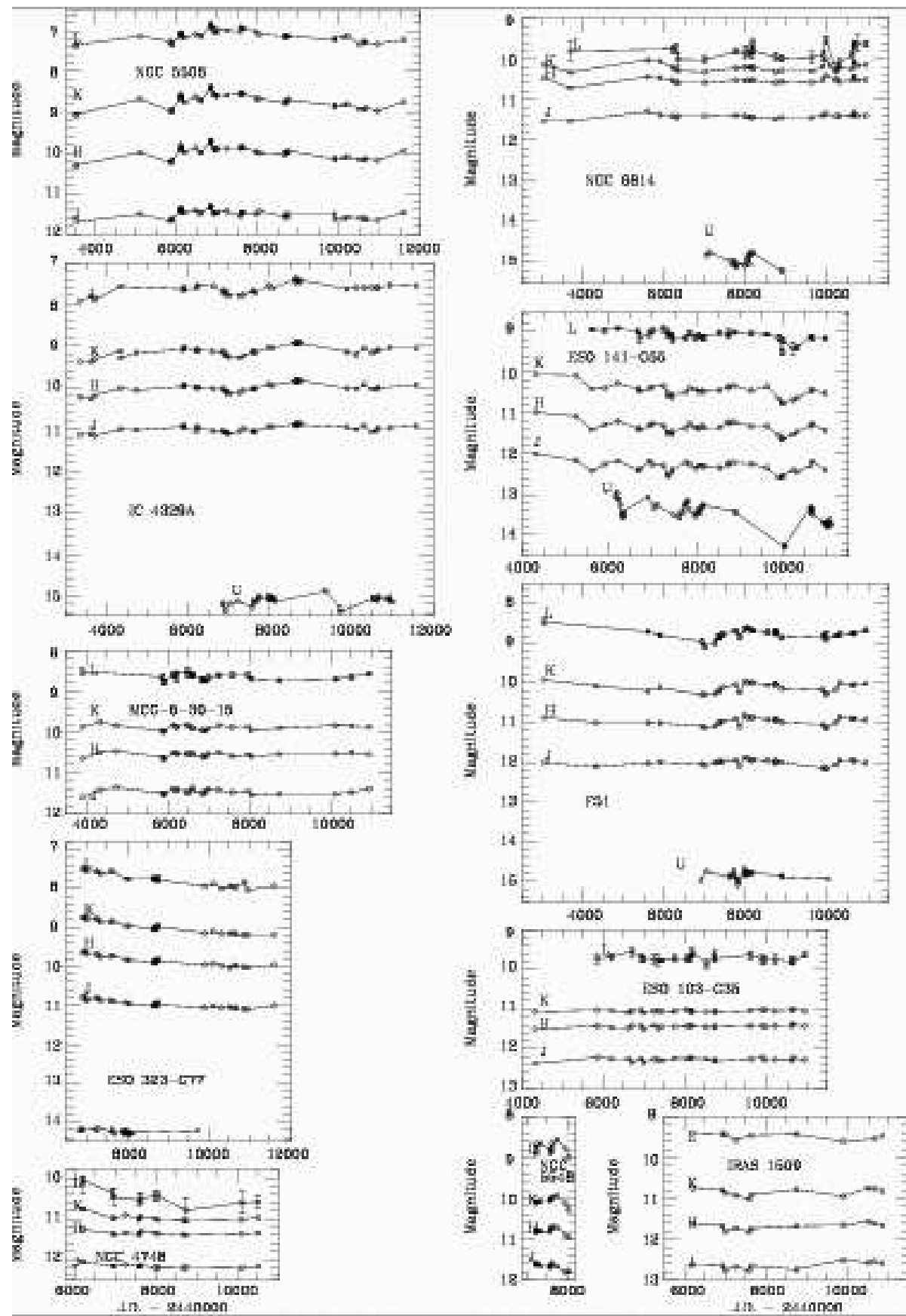


Figure 2. (c) Light curves for Seyfert galaxies

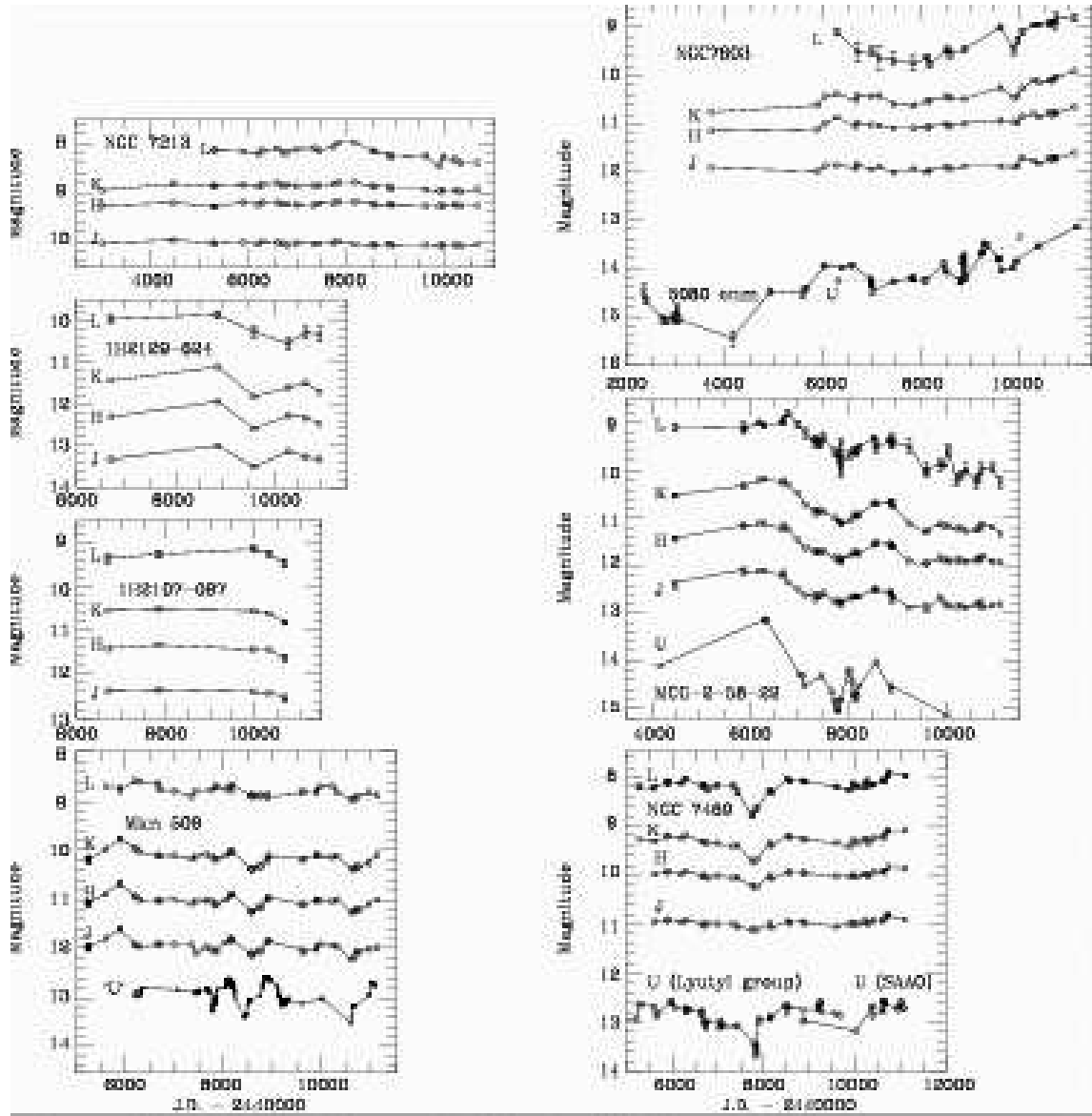


Figure 2. (d) Light curves for Seyfert galaxies

The colours from Table 3 have been plotted in a histogram (fig 3). Those with errors in excess of 0.4 mag have been omitted.

There is a strong tendency for the colour temperatures to clump at particular values. The best-determined colours are $H - K$, whose histogram peak at 1.06 corresponds to a temperature around 1600K, believed to be the highest temperature at which dust can exist without sublimation. These wavelengths may be the least contaminated by the tail of the nuclear ultraviolet continuum or an extra dust component. Taking only galaxies with errors in $H - K < 0.2$, the average colour in the 0.95, 1.05 and 1.15 columns of the histogram is $H - K = 1.056 \pm 0.016$.

In $J - H$, the typical colour temperature is around 2000K. It is likely that the tail of the ultraviolet component contributes to the J band ($1.25\mu\text{m}$) more than to the H ($1.65\mu\text{m}$), leading to an apparently hotter colour. This possibility is considered in detail for NGC 3783, for which $UBVRI$ data are available, by Glass (1992). In NGC 3783

the contribution to the J band from the extrapolated UVB flux is nearly equal to the flux from the short-wavelength tail of the blackbody radiation from dust at 1500K.

In $K - L$, the colour temperature is lower, about 1300–1400K, and may represent dust slightly further from the nucleus than that which predominates in H and K . It is possible that there is a series of zones, proceeding outward from the nucleus, with decreasing dust temperatures. It is interesting to note that an optically thick spherical dust shell having a radius of 470d (as measured for Fairall 9) and a temperature of 1400K would have an L -band luminosity of $3 \cdot 10^{24} \text{W Hz}^{-1}$. This is about 8 times the observed luminosity given in table 1. Fairall 9 has $U - B \sim -0.85$, indicating that there is almost no circumnuclear absorption along the line of sight. Thus part of the factor of 8 may result from a dust distribution which is not spherical but possibly toroidal.

Table 3. Slopes of the variable components of Seyfert galaxies, expressed as colours.

Name	H/J	K/H	L/K
III Zw 2	0.96 ± 0.11	1.19 ± 0.11	1.62 ± 0.21
Tol 0109-38	1.76 ± 0.32	1.35 ± 0.09	1.67 ± 0.30
F9	1.29 ± 0.05	1.08 ± 0.04	1.20 ± 0.06
NGC526a	1.68 ± 0.10	1.31 ± 0.04	1.67 ± 0.05
NGC985	1.08 ± 0.24	1.03 ± 0.17	1.44 ± 0.19
ESO 198-G24	0.91 ± 0.09	1.01 ± 0.07	1.35 ± 0.14
NGC1068	1.79 ± 0.72	2.47 ± 0.36	2.48 ± 0.21
NGC1566	1.19 ± 0.28	0.72 ± 0.16	1.83 ± 0.11
3C120	1.06 ± 0.10	1.01 ± 0.09	1.38 ± 0.14
Akn 120	1.14 ± 0.10	0.96 ± 0.08	1.33 ± 0.11
MCG-5-13-17	0.70 ± 0.41	1.04 ± 0.23	1.63 ± 0.17
Pic A	0.42 ± 0.34	1.63 ± 0.33	5.85 ± 0.54
NGC2110	5.47 ± 0.54	0.14 ± 0.68	5.85 ± 0.54
H0557-383	1.18 ± 0.16	1.11 ± 0.15	1.68 ± 0.40
F265	0.66 ± 0.49	1.16 ± 0.44	5.85 ± 0.54
IRAS09149-6206	2.28 ± 1.05	1.00 ± 0.30	1.22 ± 0.54
NGC2992	1.25 ± 0.12	1.27 ± 0.06	1.65 ± 0.05
MCG-5-23-16	1.28 ± 0.34	1.32 ± 0.16	1.97 ± 0.13
NGC3783	0.96 ± 0.07	1.04 ± 0.05	1.35 ± 0.08
H1143-183	0.75 ± 0.09	0.70 ± 0.09	1.22 ± 0.32
I Zw 96	1.32 ± 0.33	0.08 ± 0.22	5.85 ± 0.54
NGC4593	1.31 ± 0.21	0.98 ± 0.10	1.55 ± 0.10
NGC4748	0.69 ± 0.37	1.19 ± 0.23	1.63 ± 0.14
ESO 323-G77	1.40 ± 0.14	1.07 ± 0.08	1.28 ± 0.10
MCG-6-30-15	0.87 ± 0.32	0.92 ± 0.26	1.68 ± 0.39
IC4329A	1.33 ± 0.14	1.04 ± 0.09	1.51 ± 0.14
NGC5506	2.00 ± 0.16	1.42 ± 0.08	1.35 ± 0.10
NGC5548	1.08 ± 0.40	0.94 ± 0.23	1.79 ± 0.39
IRAS15091-2107	0.94 ± 0.32	1.13 ± 0.30	1.05 ± 0.80
ESO 103-G35	0.62 ± 0.70	-0.09 ± 0.58	5.85 ± 0.54
F51	1.37 ± 0.20	1.11 ± 0.13	1.39 ± 0.17
ESO 141-G55	1.06 ± 0.09	1.02 ± 0.07	1.39 ± 0.17
NGC6814	1.20 ± 0.35	0.87 ± 0.15	1.07 ± 0.12
Mkn 509	0.96 ± 0.08	0.97 ± 0.07	0.49 ± 0.19
1H2107-097	1.02 ± 0.25	1.04 ± 0.19	1.06 ± 0.39
1H2129-624	1.35 ± 0.17	0.96 ± 0.11	1.22 ± 0.19
NGC7213	1.10 ± 0.70	1.17 ± 0.32	1.48 ± 0.20
NGC7469	1.22 ± 0.17	1.15 ± 0.10	1.31 ± 0.11
MCG-2-58-22	1.04 ± 0.04	1.13 ± 0.03	1.30 ± 0.04
NGC7603	1.21 ± 0.12	1.16 ± 0.06	1.52 ± 0.07

6.1 Reddenings estimated from the variable components

It is noticeable that the variable part of the flux from the Seyfert 2 galaxy NGC1068 is much redder in $H - K$ and $K - L$ than the average for Seyferts as a whole. This is an indication that its nucleus is highly obscured, with $E_{H-K} = 2.47 - 1.056 = 1.414 \pm 0.37$, or $E_{B-V} = 7.6 \pm 2.0$ ($A_V = 23 \pm 6$) for a normal galactic extinction law (see also Glass, 1997b). In the J band its variation is minimal as almost no nuclear J flux can penetrate the dust barrier: the $J - H$ colour of the variable part cannot be determined precisely enough to be useful.

Five other galaxies besides NGC1068 have $H - K$ colours of their variable components which stand out from the average of 1.056 ± 0.016 in Fig 3. NGC5506 has $E_{H-K} = 1.42 \pm 0.08 - 1.056 \pm 0.016$ or 0.364 ± 0.08 . For the galactic extinction law given above and taking $E_{B-V} = 0.33$ for $A_V = 1.0$, NGC5506 would have $E_{B-V} = 2.0 \pm 0.4$. Similarly, for NGC526a, we have $E_{B-V} = 1.37 \pm 0.22$, for MCG-5-23-16, $E_{B-V} = 1.4 \pm 0.9$ and for NGC2992 $E_{B-V} = 1.2 \pm 0.3$.

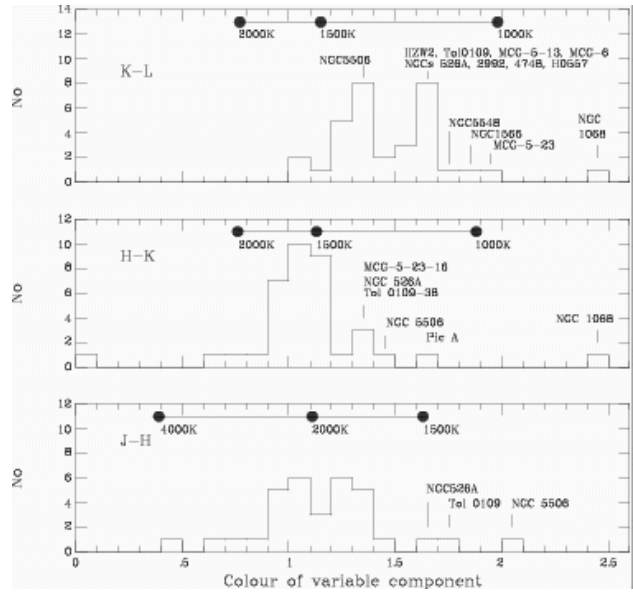


Figure 3. Distribution of infrared colours of the variable components of Seyfert galaxies. Blackbody colour temperatures are shown at the tops of each panel. Measurements with errors ≥ 0.4 have been omitted.

These values, though not very precise, are generally higher than Maiolino et al (2001) report for the same galaxies by applying the galactic extinction law to the broad H lines and may lend some support to their conclusion that the extinction law (which they discuss in terms of E_{B-V}/N_H) in the vicinity of active galactic nuclei is anomalous, i.e. that $A_V/E_{B-V} > 3.03$, the standard galactic value. The fifth galaxy, not included in Maiolino et al (2001), is Tol 0109-36 with $E_{B-V} = 1.6 \pm 0.5$.

7 CONSTANT FLUX COMPONENT

It is reasonable to assume that the flux in the 12 arcsec diameter aperture has components other than the variable one, presumed here to be from radiation by hot dust. In the simplest model it is required that this remnant flux should be ‘ordinary’ or inactive galaxy, i.e., a typical mixture of late-type giant stars (as seen in the near-infrared). The $J - H$ and $H - K$ colours of such galaxies are remarkably independent of spectral type (Glass, 1984). The effect of relativistic K-corrections have been estimated from $K_{J-H} = 0.5z$, $K_{H-K} = 3.0z$, $K_{K-L} = -1.4z$ (see Frogel et al, 1978; Longmore & Sharples, 1982; Griersmith et al, 1982) and used to predict the colours of such a component in any of the present sample.

Returning to the flux-flux plots, Figs 4a-f, 6 and 7, if nuclear activity were to cease altogether, the lowest point the fluxes could reach would be given by the intersection of the observational line with the locus of inactive galaxy flux. It is thus possible to separate the variable and fixed components independently of model surface brightness profiles.

7.1 Underlying galaxy component

If there were no other components besides ordinary galaxy and the variable source present in the 12-arcsec aperture, it would be expected that the fluxes derived from the intersections in each panel should agree with each other; i.e., that the H flux of underlying galaxy from the J vs H flux-flux plot should agree with the H flux from the H vs K plot and the K flux from the H vs K should agree with the K flux from the K vs L plot. However, the accuracy with which the points of intersection can be determined is limited by how well the slope of the variable component is known and by the extent to which the observed line must be extrapolated to meet the underlying galaxy. Further, in the J vs H plot, the accuracy is also affected by the fact that the regression line is usually almost parallel to the underlying galaxy line.

Some galaxies have solutions for H and K that are reasonably consistent. These objects are usually of low luminosity with variable fluxes that are much smaller than the underlying galaxy components, though tending to be a larger fraction at the longest wavelength. Some idea of the errors to be expected in the determination of the points of intersection can be obtained by plotting the regression lines for the observed points with slope increased by $\pm 1\sigma$ and hinged about the average flux levels.

The flux-flux diagrams also reveal that some of the most luminous members of the sample, such as H0557-383, H1143-182 and Mkn509, have almost no normal galaxy contribution to the fluxes in the 12 arcsec diameter aperture; i.e., they are essentially QSOs.

7.2 Other constant components

Most of the Seyferts in the sample cannot be resolved into a variable component and a simple underlying standard inactive galaxy.

Taking F9 (Fig 5) as an example, which will be discussed below in more detail, the H flux of the intersection in the J vs H diagram is 18 mJy, whereas it is only 10.2 mJy in the H vs K diagram. Similarly, the K flux of the intersection is 10.2 mJy in the H vs K and -21 mJy in the K vs L diagrams, the latter being clearly unphysical. It will be seen that these discrepancies can be resolved by postulating the existence of a component with associated cool dust that contributes to the fixed flux, increasing with wavelength.

Another example of this kind is NGC 7469, which was discussed in detail by Glass (1998). A circumnuclear ring exists in this galaxy and appears to constitute a non-variable contribution in addition to the ordinary galaxy stellar component. The ring has been measured at high spatial resolution in JHK by Genzel et al (1995), so that its contribution is known.

8 PARAMETERIZATION OF THE NUCLEAR ACTIVITY

Because of the linear relations between fluxes at different wavelengths, the position of a measured point along the regression line in a flux-flux diagram (see fig 5) can be taken as a measure of the activity at the time. We can define an activity parameter A which rises from 0 at the point where

the regression line crosses the locus of the ordinary galaxy component to 1 at the maximum of the observed flux. An error can be estimated for A by determining the points at which the $\pm\sigma$ regression lines intersect with the same locus. The error can be large if there are only a few observational points or if the regression line is almost parallel to the ordinary galaxy line. Such is often the case for the H , J diagram.

For several galaxies, the errors are small and the values of A found from all three diagrams agree reasonably well. These are well-observed objects whose constant component appears to be pure inactive galaxy.

In the case of those galaxies where an extra constant component seems to be present, the intersections in the L , K diagram are lower down than expected, and sometimes at unphysical values, because the extra component is cool and causes a displacement of the longer-wavelength fluxes (plotted always along the x-axis) to the right. A self-consistent picture of the different contributions can often be derived by starting with the H vs J or the K vs H regressions, according to the probable errors, and estimating the effects of the extra component, followed by iterating. Because of its low temperature it has relatively little effect at shorter wavelengths. Based on the well-observed galaxy F9, the ratio of $L : K : H$ fluxes are about 4 : 1 : 0, corresponding to a cool dust component of ~ 850 K. This galaxy is discussed in detail in section 9.3. Its J and H fluxes lead to a value of A at the lowest level of activity of about $11 \pm 3\%$ of the maximum observed values.

Table 4 gives the value of A based on the H vs K diagrams for suitable candidates, together with the underlying galaxy flux in the 12 arcsec measuring aperture at K and an estimate of the excess cool component, if present, at L .

9 COMMENTS ON INDIVIDUAL GALAXIES

Many of the galaxies observed during this programme are the subjects of extensive studies only a few of which will be referred to.

9.1 III Zw 2

This is one of the galaxies in which variations were found by Lebofsky & Rieke (1980). At the time of their work (1978-79) it was at the high end of its luminosity range. Their photometry falls (after correction for reddening) close to the regression lines derived from the present work. The infrared increase they observed was attributed to a previously noted increase in its optical-UV radiation, providing early evidence for the dust reverberation model.

The slope of the regression in the K vs L diagram may have changed with time in the sense that the L flux is continuing to decrease even though the K flux has bottomed out. This may be a reflection of a very long-term decrease in the L flux, arising from relatively distant dust, following a protracted decline in UV activity since the time of the Lebofsky & Rieke work. See also NGC 2992, MCG-2-58-22 and NGC 7469 below.

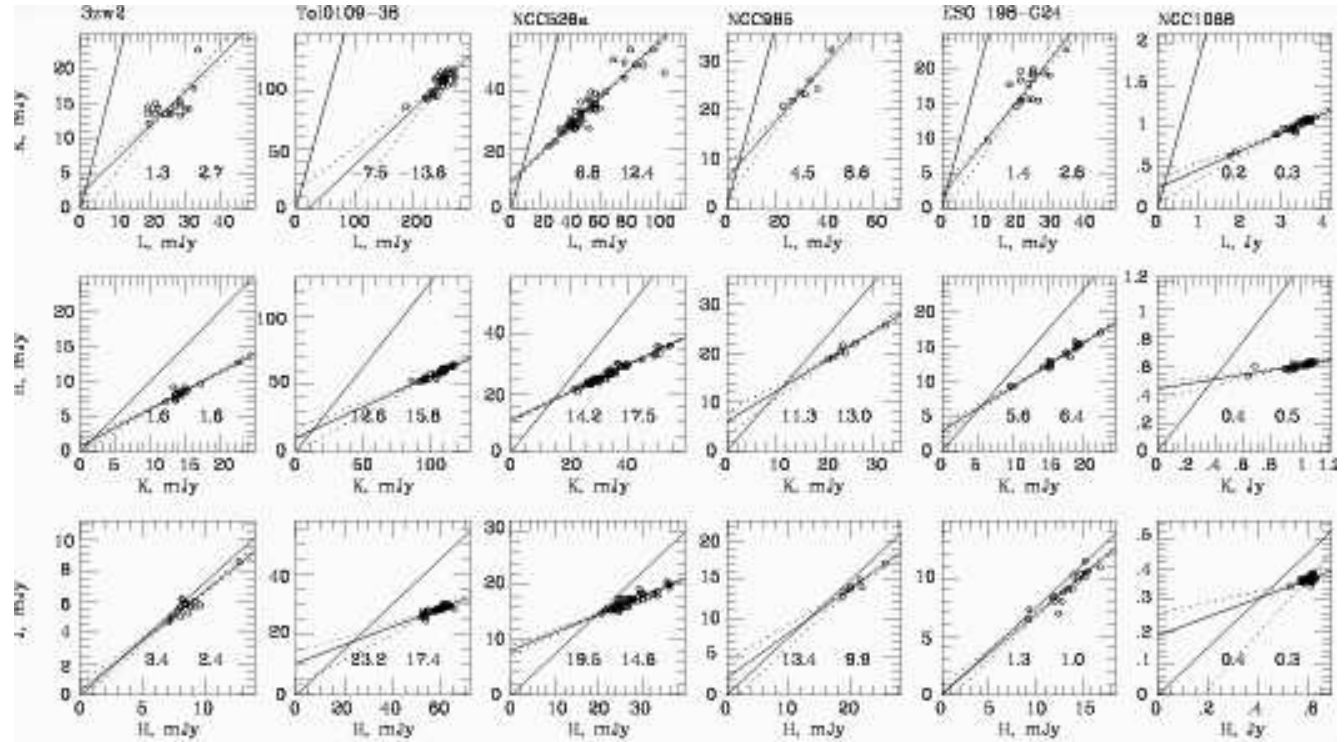


Figure 4. (a) Linear flux-flux diagrams of galaxies with variable nuclei. The ranges of the abscissas and ordinates have been chosen to have the same ratios from galaxy to galaxy in order to facilitate the comparison of slopes. The regression lines are shown (solid) with companion lines having slopes differing by $\pm\sigma$ (dotted). Also given for each diagram is a line representing the colour of an average 'ordinary galaxy' at the same redshift. The coordinates of the intersection points are given. If the sole non-variable content is ordinary galaxy, the H coordinate of the intersections should be the same for the J vs H and H vs K diagrams. Similarly for the K coordinates in the H vs K and K vs L diagrams. The fact that this is not usually the case implies that a cool dust component may also be present (see text). Note that error bars have not been plotted, but errors may be judged from Fig. 1.

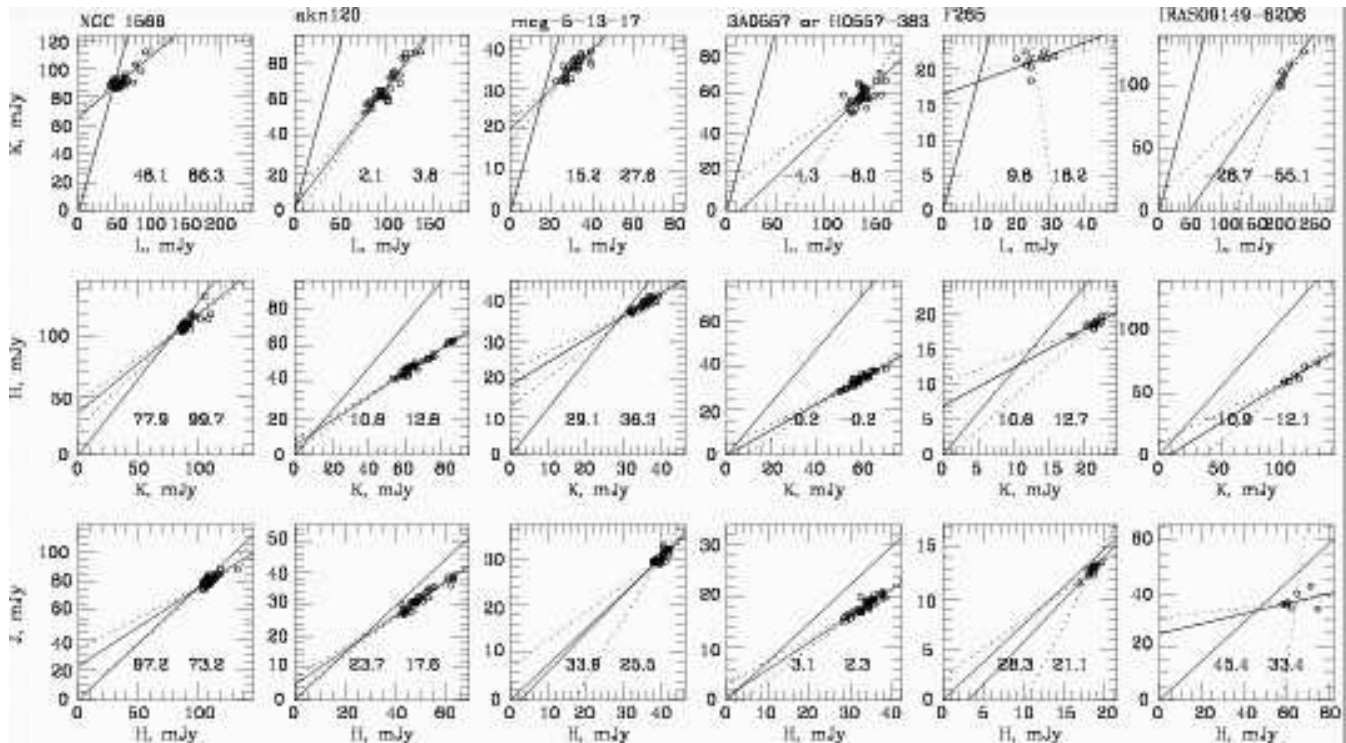


Figure 4. (b) Linear flux-flux diagrams (contd.).

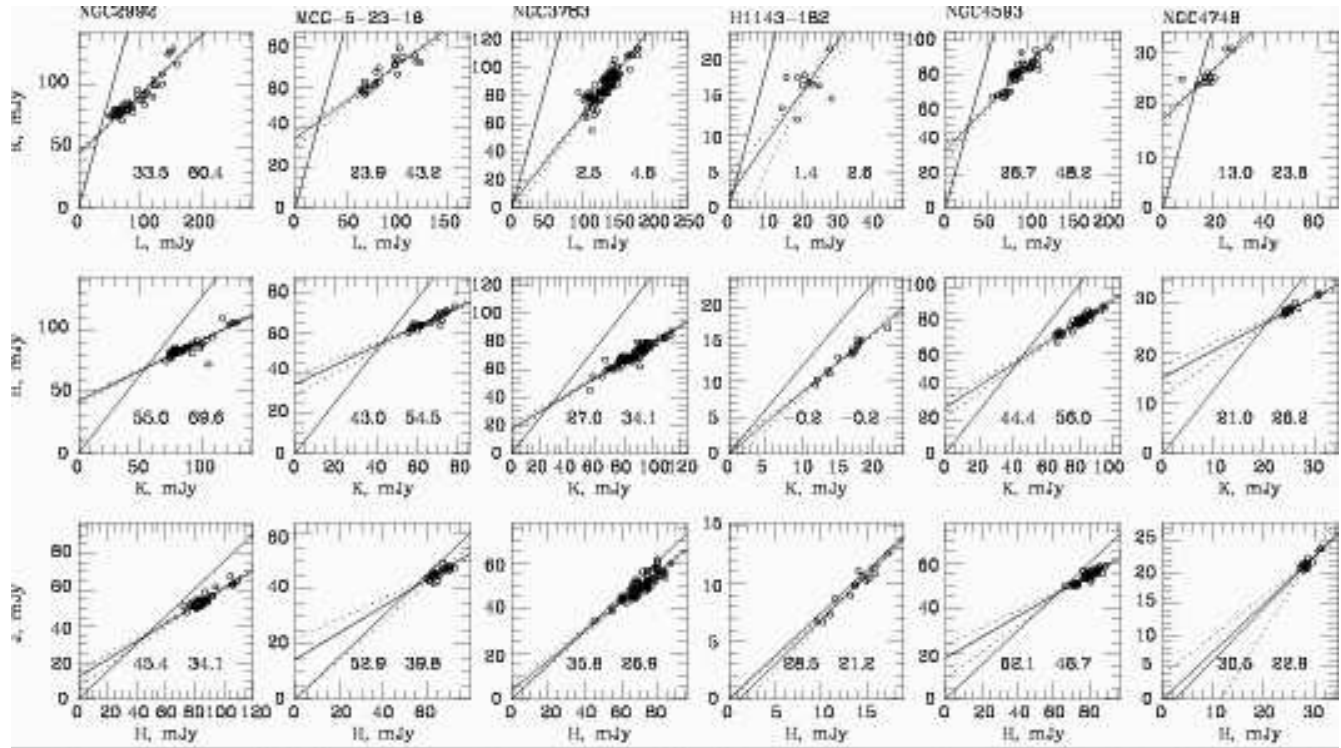


Figure 4. (c) Linear flux-flux diagrams (contd.)

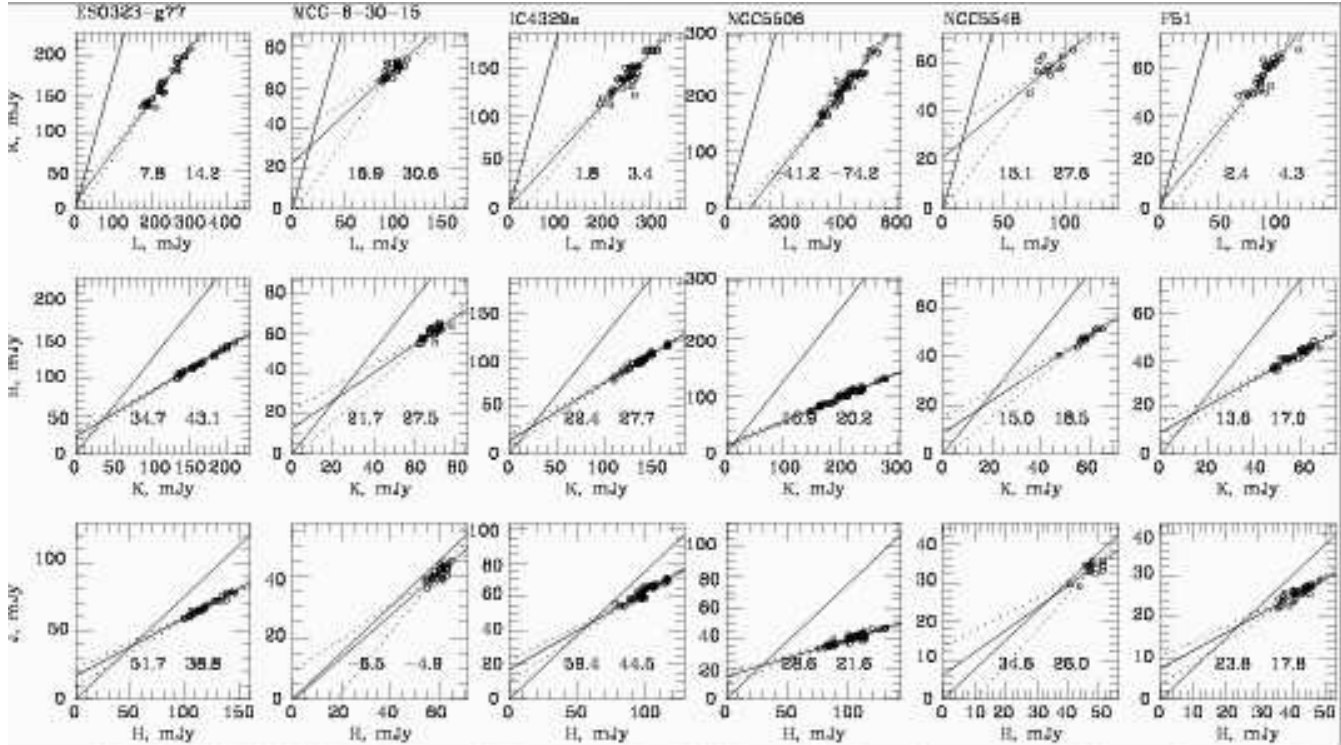


Figure 4. (d) Linear flux-flux diagrams (contd)

9.2 Tol 0109-28

This Seyfert 2 galaxy has shown very little activity. The colours of its variable components are considerably redder than average, suggesting strong nuclear reddening. There appears to be a delay of about 100d between J and L .

9.3 Fairall 9

The data on Fairall 9 yield the best argument so far for the dust reverberation model. The delay of ~ 400 d found by Clavel, Wamsteker & Glass (1989) between the IUE continuum and the L -band light curve remains the strongest

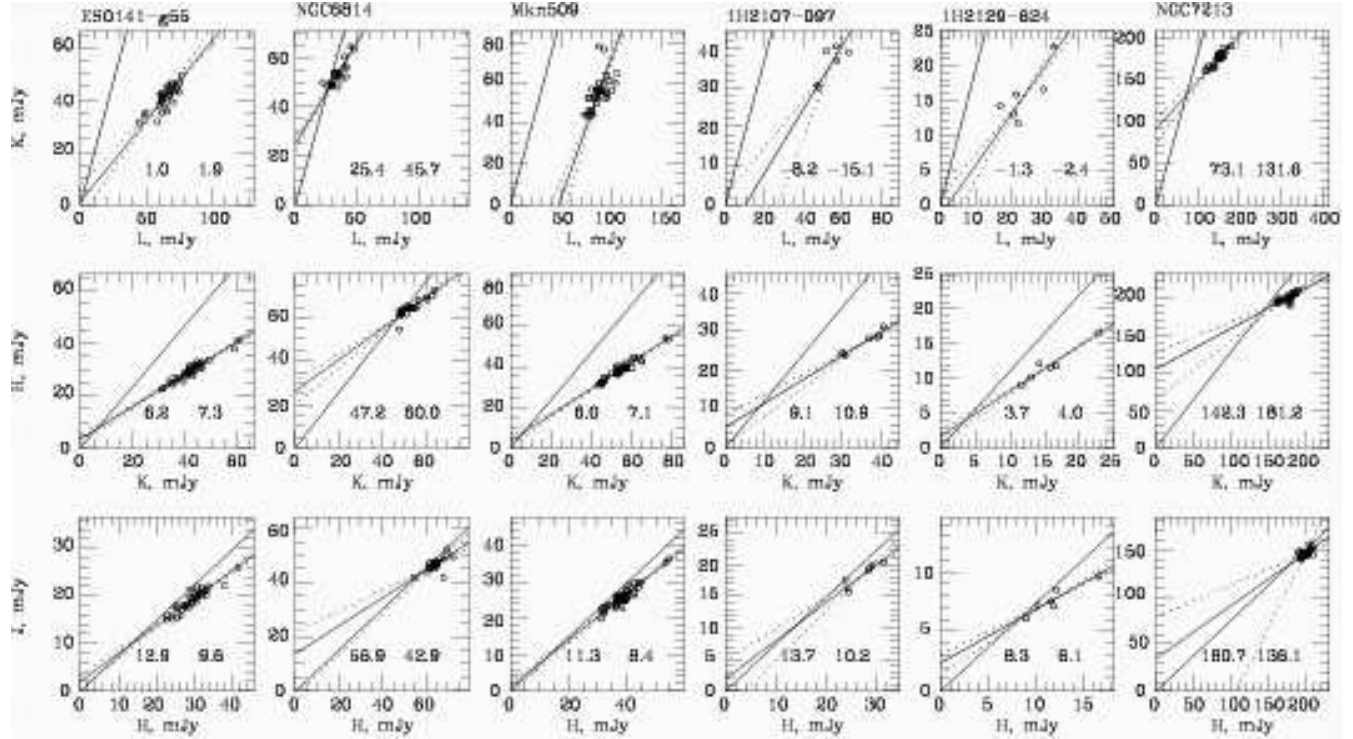


Figure 4. (e) Linear flux-flux diagrams (contd)

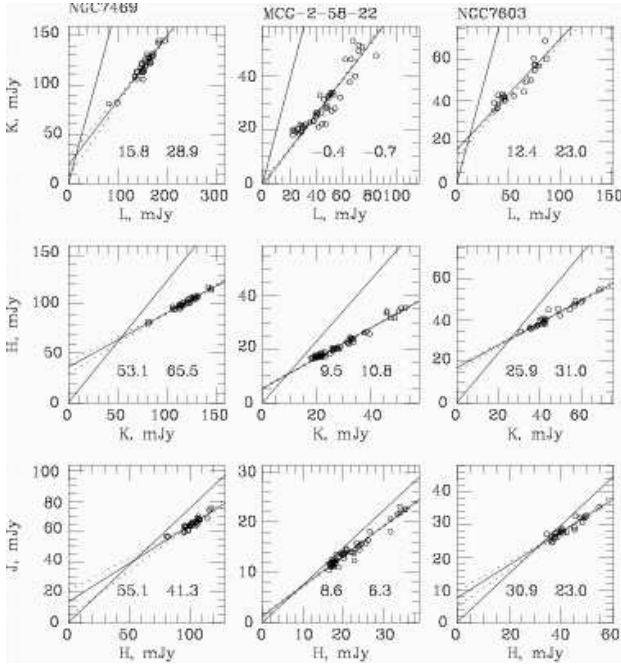


Figure 4. (f) Linear flux-flux diagrams (contd.)

evidence for the dust reverberation model. Monitoring has continued at SAAO in the U band and a delay is still seen in the infrared response. The SAAO U data are shown in Fig 1. Variations seen in the new U data are found to precede those at L by 470d. The lag between J and L for the entire data set is found to be 370d.

Fig 5 shows the flux-flux plots for F9, together with

the ‘activity parameter’, A . In the J vs H diagram, the point corresponding to the level of activity the lowest flux comes closer to the ‘ordinary galaxy’ line than in the other two diagrams. We now assume that the point of intersection of the two lines, $(H, J) = (18 \pm 2, 13.5 \pm 2)$, represents pure galaxy and an activity of $A = 0$. The minimum observed activity, as a proportion of the maximum, is then $A = 0.11 \pm 0.03$.

Using the minimum and maximum levels of A , we can estimate the points on the H vs K diagram where A would be zero, namely at $(K, H) = (22, 18)$, with correlated uncertainties of about ± 2 mJy in each coordinate. It is clear that in Fairall 9, as well as many other galaxies, this point does not coincide with the intersection of the regression line and the ordinary galaxy line. Instead, the position of the point at $(22, 18)$ can be regarded as the sum of an ‘ordinary galaxy’ component of $(16, 18)$ and an underlying constant component with $F_H \sim 0$ (see next paragraph) and $F_K = 6 \pm 2$ mJy.

Similarly, for the K vs L diagram, the position of the point corresponding to $A = 0$, namely $(L, K) = (50, 24)$ can be regarded as the sum of an ordinary galaxy component of $(9, 16)$ with an underlying constant component of $(41, 8)$. This corresponds to a $K - L$ colour of 2.42, or a blackbody temperature of ~ 850 K. The $H - K$ colour for this temperature of blackbody is 2.4, which would imply an H flux only about 18% of the K flux, or about 1.4 mJy. This is sufficiently close to the estimated flux of 0 to be acceptable.

Barvainis (1992) made a detailed reverberation model of Fairall 9, based on the data presented by Glass (1986) and Clavel, Wamsteker & Glass (1989). It should be noted that information from a well-sampled IUE UV light curve, contemporary with the infrared data, was available for this

Table 4. Further results from flux-flux diagrams: Activity parameters and underlying galaxy components (within 12 arcsec diameter aperture) for galaxies with sufficient variability and sufficient data.

Galaxy	A_{min}^{HK}	K_{gal} (mJy)	comments
III Zw 2	$0.49^{+0.1}_{-0.06}$	<3	VS
Tol 0109-38	$0.70^{+0.06}_{-0.09}$	<20	
F9	$0.11^{+0.04}_{-0.02}$	16 ± 2	
NGC526a	$0.056^{+0.025}_{-0.027}$	14 ± 2	no strong CE
ESO198-G24	$0.45^{+0.1}_{-0.1}$	5.6 ± 1	no strong CE
NGC1068	$0.33^{+0.05}_{-0.02}$	390 ± 50	CE = 0.25Jy
NGC1566	$0.27^{+0.29}_{-0.08}$	87 ± 5	
3C120	0.5	~ 10	CE = 16 mJy
Akn120	$0.58^{+0.09}_{-0.04}$	~ 11	CE = 35mJy
MCG-5-13-17	$0.26^{+0.18}_{-0.14}$	29 ± 5	
H0557-383	0.72	<7	
NGC2992	$0.20^{+0.04}_{-0.02}$	55 ± 2	VS
MCG-5-23-16	$0.35^{+0.05}_{-0.05}$	43 ± 2	
NGC3783	$0.28^{+0.04}_{-0.04}$	32 ± 5	CE = 32 mJy
PKS1143-182	$0.55^{+0.04}_{-0.06}$	<2	
NGC4593	$0.41^{+0.07}_{-0.03}$	46 ± 4	no strong CE
NGC4748	$0.28^{+0.10}_{-0.06}$	21 ± 2	no strong CE
ESO323-G77	$0.56^{+0.04}_{-0.10}$	36 ± 10	no strong CE
MCG-6-30-15	$0.74^{+0.08}_{-0.09}$	<30	
IC4329A	$0.37^{+0.17}_{-0.08}$	~ 50	CE = 97 mJy
NGC5506	0.43	~ 27	CE = 140 mJy
F51	$0.45^{+0.16}_{-0.10}$	~ 17	CE = 23 mJy
ESO141-G55	0.32	~ 12	CE = 20 mJy
NGC6814	~ 0	47 ± 2	no strong CE
MKN 509	0.51	~ 23	CE = 40
NGC7213	$0.74^{+0.08}_{-0.09}$	140 ± 10	no strong CE
NGC7469	0.19	~ 58	CE = 41
MCG-2-58-22	0.15	~ 11	CE = 15; VS
NGC7603	$0.13^{+0.03}_{-0.03}$	26 ± 1	no strong CE, VS

Notes:

CE denotes cool excess component at L , in mJy.

VS denotes variable K vs L slope

Values without quoted errors are the (approximate) results of iterative solutions.

Absorption within the Milky Way galaxy has been allowed for.

galaxy. From Fig. 2 of Glass (1986) he took the underlying galaxy contribution in a 12 arcsec diameter aperture to be 14, 19, 17 and 9 mJy at $JHKL$ respectively. These figures are close to the 13.5, 18, 16 and 9 mJy used in the work just described. From fits of his dust model, Barvainis concluded that there must be a ‘fourth component’ of flux that is constant with time. He found for this flux the $JHKL$ values 1.5, 3.7, 9.0 and 37mJy respectively, arising from quiescent dust at about 800K or a power law with $\alpha = -3$. His deduction is consistent with the results found here, i.e. that the fourth component has $F_K = 8$ and $F_L = 34$ mJy. The present method gives no information as to F_J and F_H as they are tacitly taken to be zero but, if the source is dust at 800K, we have seen that the fluxes at these wavelengths will be small.

9.4 NGC 526A

This object appears heavily obscured in visible light and its variable component is significantly redder than average. There is some evidence for a delay between J and L of 200 ± 100 days.

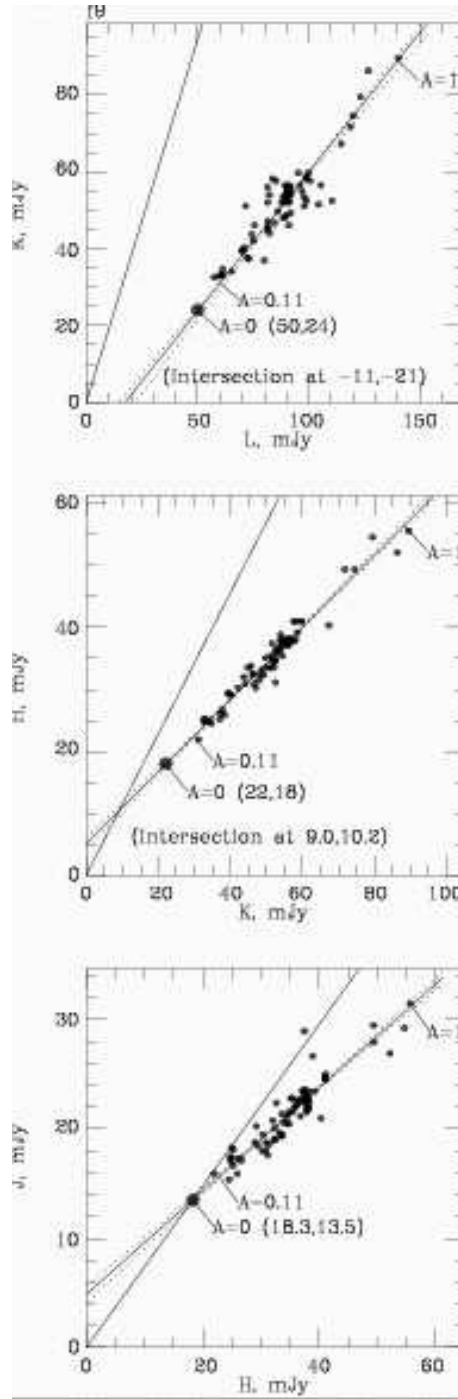


Figure 5. Flux-flux diagrams for Fairall 9 observed through a 12-arcsec diameter aperture, including information on the ‘Activity parameter’. A is taken to be 1 at the maximum observed level and to be zero at the place in the H vs J diagram where the regression line intersects with the ordinary galaxy line. The lowest observed fluxes in the same diagram have $A = 0.11 \pm 0.03$. The position of $A=0$ in the other two diagrams can be estimated from the highest and lowest observed fluxes. From these the contribution of an additional non-varying component of flux can be estimated (see text).

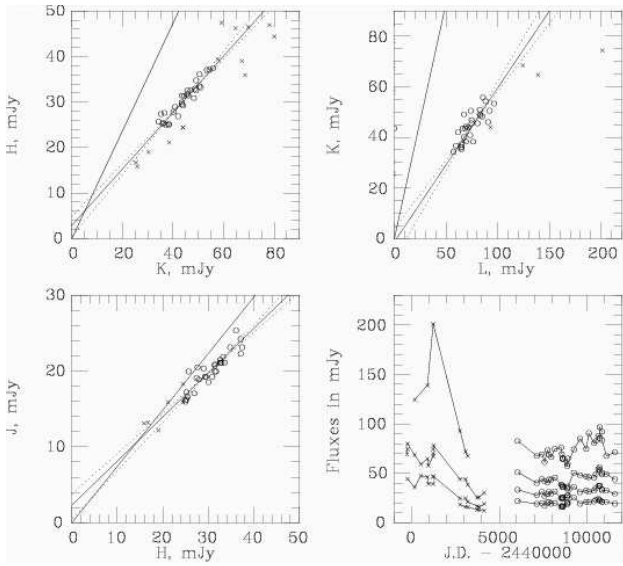


Figure 6. Flux-flux diagrams and light curves for 3C120. The crosses are data from other authors. Note that the errors on the early L data range from 15 to 30 percent. The early data (shown by crosses) were not used in the determination of the regression lines.

9.5 ESO 198-G24

A large visual range was found for this galaxy by Winkler et al (1992).

9.6 NGC 1068

The archetype S2 galaxy, NGC 1068 has been discussed in detail by Glass (1995). The $J - H$ colour of its variable component is not well-determined, but the $H - K$ and $K - L$ colours are by far the reddest of the sample.

9.7 NGC 1566

A detailed discussion of the event around JD 2447000, as observed at many wavelengths from the x-ray to the IR, was given by Baribaud et al (1992). A time lag of 2 ± 1 months was found between the UV and the IR. This result was criticised by Oknyanskij & Horne (2001), who find that the delay is consistent with 0 and is less than 20d.

9.8 3C 120

Lebofsky & Rieke (1980) reported a decline in the K flux of 3C 120 from levels of 64–71 mJy, that had been observed in 1970–1972 by Penston et al (1974), to ~ 24 mJy in 1978. This decline took at least three years. In the present work the (not dereddened) K flux varied from 32 to 47 mJy. Only three galaxies in the present sample have shown such large changes. However, the case for 3C 120 seems to be well corroborated and is almost certainly real. The Penston et al and Lebofsky & Rieke values are plotted with the present data in Fig 6 as crosses. The fluxes tend to lie quite close to the regression lines shown except at L , where the Penston L values seem too bright. However, the standard errors of his measurements were quite high.

Long-term B light curves of 3C 120 have been presented by Hagen-Thorn et al (1997) and Clements et al (1995), in which a decline over the years 1973 to 1978 is clearly seen.

A cross-correlation analysis between J and L shows that the longer wavelength emission is delayed by about 160 days compared to the shorter.

9.9 Akn 120

Akn 120 has been monitored in the visible region at SAAO by Winkler et al (1992), Winkler (1997) and in a service observing programme at SAAO under the control of Dr D. Kilkenny.

It has also been observed extensively by Doroshenko & Lyuty (1999), who found that the $U - B$ colour of its variable component did not remain constant during two episodes of fading.

A delay of about 315 days was found between U and L , but between J and L only ~ 60 d was found. Clavel, Wamsteker & Glass (1989) found that the delay between U and the near-IR wavelengths tended to be increase with wavelength in F9. Uneven sampling could also play a part in the seeming discrepancy.

9.10 MCG-5-13-17

Visible-region photometry from Winkler et al (1992) & Winkler (1997) is also shown. The U data are insufficient for cross-correlation purposes.

9.11 H0557-383

This is one of the most luminous galaxies in the sample and it shows clear evidence for a delay of about 305d between variations at J and L (See also Fig 1).

9.12 F265

U points from Winkler et al (1992) and Winkler (1997) are shown.

9.13 IRAS09149-6206

This is the most luminous galaxy in the sample but unfortunately there are insufficient data to determine a lag.

9.14 NGC 2992

This galaxy showed some form of outburst, much more luminous than any normal supernova, at around JD2447200. The cross-correlation programme described here does not yield a significant delay between J and K . However, Oknyanskij & Horne (2001) find 18 ± 10 d between J and K and 84 ± 30 d between J and L . The programme used here gets a delay of about 35d between J and L .

The K vs L diagram shows some curvature instead of a linear relation. Glass (1997a) mentioned that the time constant for the decay of the outburst at L is considerably longer than that for K .

9.15 MCG-5-23-16

This galaxy shows little variation at J and no significant evidence for delays.

9.16 NGC 3783

The data now presented stretch about 3000 days beyond those of Glass (1992) which suggested the existence of a delay of about 80 days between U and L . The data now available now suggest a delay of about 190d. It should be noted, however, that the sampling is rather inadequately spaced.

9.17 NGC 4593

Oknyanskij & Horne (2001) conclude from the data of Santos-Ll  o et al (1994) that there is a delay of 36 ± 15 d between the J and L variations. The present analysis yields 55d.

9.18 ESO323-G77

The nucleus of this bright Seyfert 1 galaxy is partially obscured and shows visible-light polarization explicable by scattering off dust close to a torus (Schmid, Appenzeller & Burch, 2003). In the infrared it shows a slow decline over ~ 5000 d, by about 0.2 mag at L and about 0.1 mag at J .

9.19 MCG-6-30-15

This well-known x-ray galaxy has shown only modest variations in the IR and its flux variation gradients cannot be determined very accurately. A delay of about 34d between J and L is indicated.

9.20 IC4329A

This has a partially obscured nucleus, very faint at visible wavelengths (Winkler et al, 1992). There is a suggestion of a delay of between 33 and 85d between J and L .

9.21 NGC 5506

This is a heavily obscured nucleus, with colours of its variable part much redder than average in $J - H$ and $H - K$. A delay of about 25d between J and L may be present.

9.22 ESO 103-G35

Shows no significant variability.

9.23 F51

A high-polarization Seyfert 1 galaxy, similar to ESO 323-G77. The infrared colours are not noticeably redder than average. There is a delay of about 15d, probably not significant, between J and L . The cross-correlation of U with L does not yield a sensible result, possibly because of the poorer sampling in U .

9.24 ESO141-G55

Cross-correlation between U and L gives 230d, while between J and L a delay of ~ 160 d is found.

9.25 NGC 6814

This is a Seyfert with nearly ‘ordinary’ colours much of the time. Oknyanskij & Horne (2001) report an upper limit for the delay between U and K of 15d, based on work by B.O. Nelson. The present data give ~ 35 d.

9.26 Mkn 509

For the interval JD 2447415–9323, Carone et al (1996) have published visible-region spectrophotometric data which includes F_λ (5110Å) data. It is found that these data, converted to a magnitude scale and assigned a suitable zero point, fit well with the U -band data obtained at SAAO by Winkler et al (1992), Winkler (1997) and as part of the service programme. Further data by Doroshenko (1996) is also in good agreement. A hybrid ‘ U ’ light curve has been constructed from these data and is shown in Fig 1.

The L band output appears to be heavily smoothed compared to the U , J , H and K . The delay between U and L is poorly defined but seems to be about 60d. However, the K flux lags the U by about 100 days. It is possible that the geometry of the dust shell smears out the L response. It is also the case that there was no infrared monitoring just after the UV outbursts at JD2448100 and 2448800, when the long wavelength emission might have been expected to peak.

The K vs L diagram of Mkn509 shows an atypical slope for the regression line which makes the $K - L$ colour of the variable component much bluer (0.49 ± 0.23) than average. If the two brightest K points are omitted, the slope is changed significantly and $K - L$ has a more typical value, viz 1.13 ± 0.19 . However, no obvious mistake can be found in the photometric record.

Carone et al (1996) note that the response of H_β and $HeII$ to the continuum variations show lags of ~ 80 and ~ 60 d respectively; these delays are unusually long.

9.27 NGC 7469

Oknyanskij & Horne (2001) have taken the data of Glass (1998) and cross-correlated it with published and unpublished U photometry (e.g. Doroshenko, Lyutyi & Rakhimov, 1989; Chuaev, Lyutyi & Doroshenko, 1990), finding that there are delays of 52 ± 15 d at K and 60 ± 10 d at L . The present data, using only the published U photometry, yield, with lower significance, a delay between U and L of ~ 21 d and between J and L of ~ 40 d. The Oknyanskij & Horne (2001) value should probably be preferred.

9.28 MCG-2-58-22

Four RoSat X-ray observations plotted by Kim & Boller (2002) covering JD 2448000 to 2449500 are consistent with the peak we see in the U band around JD 2448500.

This galaxy declined by over a magnitude in L between JD 2446800 and JD 2450000, with minor recoveries. The L

vs K diagram, although affected by observational scatter, seems to show a flattening out, or change of slope, as the galaxy becomes faint, in the sense that K is tending towards a constant value as L declines further. There is some indication of a similar, but less certain, trend in the K vs H diagram. The explanation may be that the hottest dust, closest to the nucleus in distance and propagation time, has already cooled in response to the shutting off of the ultraviolet component, and a cooler dust zone that contributes to the L radiation is still cooling because it is further away and takes longer to respond.

The present data suggest a delay of ~ 160 d between J and L .

9.29 NGC 7603

NGC 7603 has been monitored spectrophotometrically in the visible for 20 years by Kollatschny, Bischoff & Dietrich (2000). Their continuum flux at 5080Å is plotted in Fig. 1. The general features of the continuum variations are also seen in the infrared. Unfortunately, there was no IR coverage around the continuum peak at \sim JD 2449270. The sharp spike in continuum emission at JD2448862 does not seem to have affected the IR observation on JD 2448874. The JHK fluxes and colours at the time of the first IR observation (JD 2443719) are consistent with an ordinary underlying galaxy. From the Kollatschny et al (2000) data it is probable that the nuclear activity was then close to its lowest point.

The cross-correlation programme does not yield a useful output.

10 CONCLUSIONS

Thirty-nine of the forty-one Seyfert galaxies in this sample have shown variability during the observing programme; some of them by over one mag. These variations reflect changes in the ultraviolet output of the central engine in the same way as the visible-light continuum and spectral line observations do; i.e., after a certain time-lag.

Lags are common and most conspicuous at L , but difficult to determine accurately. Several of the lower-luminosity galaxies in the present sample have been shown to vary and to exhibit probable lags on time scales of tens of days. These will repay study with more frequent sampling. There is some suggestion that a decline in the L flux following a drop in the UV from the central engine may show a longer time constant than its counterpart at K , perhaps because of increased radial extent of the dust zone which contributes most at this wavelength.

For the most part, there are strong linear correlations between the J , H , K and L fluxes. The colours of the variable components are therefore easy to determine, provided that the variations have sufficient amplitude and the photometry is sufficiently accurate. There is a high degree of uniformity of colours among the variable components which allows an estimate of the nuclear reddening to be made in heavily reddened cases. It also clear that the near-infrared emission mechanism is the same in all Seyfert galaxies.

In many cases, the fluxes seen through the measuring aperture can be separated into variable and underlying

Table 5. Sample data table, for III Zw 2. See web version for remainder.

MJD	J	H	K	L	L_{err}
3717	13.18	12.25	11.11	9.82	.12
6695	13.61	12.55	11.41	9.86	.14
6989	13.71	12.67	11.54	10.01	.09
7436	13.60	12.70	11.63	9.95	.11
7437	13.55	12.72	11.61	10.28	.10
7342	13.55	12.68	11.65		
7842	13.54	12.74	11.67	10.32	.16
8132	13.67	12.78	11.68	10.19	.05
8172	13.59	12.69	11.62	9.91	.06
8227	13.56	12.61	11.57	10.00	.13
8529	13.79	12.86	11.67	10.43	.22
8574	13.64	12.76	11.60	10.07	.17
8576	13.75	12.75	11.67	10.10	.18
8874	13.75	12.84	11.67	10.13	.05
9966	13.84	12.89	11.79	10.41	.12
10655	13.61	12.66	11.56	10.31	.17
10742	13.64	12.61	11.69	10.00	.16
11117	13.60	12.71	11.60	10.43	.16

galaxy components without recourse to surface-brightness modelling. In a number of galaxies, a further non-variable component, probably arising from cool dust, is clearly present at L and may be modelled.

11 ACKNOWLEDGMENTS

I would like to thank Dr David Kilkenny and François van Wyk and Fred Marang, the observers on the SAAO 0.5-m service programme, for unpublished $UBVRI$ photometry. Dr Hartmut Winkler (VISTA University) is thanked for reading an early version of the ms. Dr Chris Koen (SAAO) has helped by commenting on statistical and other questions. The referee, Dr Victor Oknyanskij, is thanked for useful comments.

REFERENCES

Baribaud T., Alloin D., Glass, I.S., Pelat D., 1992, A&A, 256, 375
 Barvainis R., 1987, ApJ, 320, 537
 Barvainis R., 1992, ApJ, 400, 502
 Carter B.S., 1990, MNRAS, 242, 1
 Carone T.E. et al, 1996, ApJ, 471, 737
 Choloniewski J., 1981, Acta Astr, 31, 293
 Chuvaev K.K., Lyutyi V.M., Doroshenko V.T., 1990, Sov. Astr. Letts., 16, 372
 Clavel J., Wamsteker W., Glass I.S., 1989, ApJ, 337, 236
 Clements S.D., Smith A.G., Aller H.D., Aller M.F., 1995, AJ, 529
 Doroshenko V.T., 1996, Astr. Letts., 22, 309
 Doroshenko V.T., Lyutyi V.M., 1999, Astr. Letts., 25, 883
 Doroshenko V.T., Lyutyi V.M., Rakhimov V.Yu., 1989, Sov. Astr. Letts., 15, 207
 Frogel J.A., Persson S.E., Aaronson M., Matthews K., 1978, ApJ, 220, 75
 Gaskell C.M., Peterson B.M., 1987, ApJS, 65, 1
 Genzel R., Weitzel L., Tacconi-Garman L.E., Blietz M., Cameron M., Krabbe A., Lutz D., Sternberg A., 1995, ApJ, 444, 129
 Glass I.S., 1984, MNRAS 211, 461
 Glass I.S., 1986, MNRAS 219, 5p (Fairall 9)
 Glass I.S., 1992, MNRAS 256, L23. (NGC 3783)
 Glass I.S., 1995, MNRAS 276, L65 (NGC 1068)
 Glass I.S., 1997a, MNRAS 257, L50 (NGC 2992)

Glass I.S., 1997b, ApSpSci, 248, 191
 Glass I.S., 1997c, Mon Notes astr Soc S. Africa, 56, 110
 Glass I.S., 1998, MNRAS 297, 18 (NGC 7469)
 Glass I.S., Carter B.S., 1989, In IAU Joint Commission Meeting
Problems of Infrared Standardisation and Extinction, ed. E.F.
 Milone, Springer, Berlin, 37
 Griersmith D., Hyland A.R., Jones T.J., 1982, AJ, 87, 1106
 Hagen-Thorn V.A., Marchenko S.G., Mikolaichuk O.V., Yakoleva
 V.A., 1997, Astr. Rep., 41, 1
 Kim C., Boller T., 2002, ApSpSci 281, 663
 Kollatschny W., Bischoff K., Dietrich M., 2000, A&A, 361, 901
 Lebofsky M.J., Rieke G.H., 1980, Nature, 284, 410
 Longmore A.J., Sharples R.M., 1982, MNRAS, 201, 111
 Maiolino R., Marconi A., Salvati M., Risaliti G., Severgnini P.,
 Oliva E., La Franca F., Vanzi L., 2001, A&A, 365, 28
 Nelson B.O., 1996, ApJ 465, L87
 Oknyanskij V.L., 2002, in Galaxies, the Third Dimension, ASP
 Conf. Ser. Vol. 282, p. 330
 Oknyanskij V.L., Horne K., 2001, in Probing the Physics of Active
 Galactic Nuclei by Multiwavelength Monitoring, ASP Conf.
 Ser. Vol. 224, p. 149
 Penston M.V., Penston M.J., Selmes R.A., Becklin E.E., Neuge-
 bauer G., 1974, MNRAS, 169, 357
 Pier E.A. & Krolik J.H., 1992, ApJ, 401, 99
 Pier E.A. & Voit G.M., 1995, ApJ, 450, 628
 Salvati M. et al, (1993), A&A, 274, 174
 Santos-Ll  o M., Clavel J., Barr P., Glass I.S., Pelat D., Peterson
 B.M., Reichert G., 1995, MNRAS 270, 580
 Schlegel D.J., Finkbeiner D.P., Davis M., 1998, ApJ, 500, 525
 Schmid H.M., Appenzeller I., Burch U., 2003, A&A, 404, 505
 Simon T., Drake S.A., 1989, ApJ, 346, 305
 V  ron-Cetty M.-P., V  ron P., 2000, ESO Scientific Report No. 19
 Winkler H., 1997, MNRAS, 292, 273
 Winkler H., Glass I.S., van Wyk F., Marang F., Spencer Jones
 J.H., Buckley D.A.H. and Sekiguchi K., 1992. MNRAS, 257,
 659

Table 6. Tol0109-38

MJD	<i>J</i>	<i>H</i>	<i>K</i>	<i>L</i>
5302	11.91	10.65	9.43	7.60
5885	11.91	10.66	9.52	7.70
6287	11.84	10.64	9.48	7.65
6664	11.80	10.52	9.36	7.63
6692	11.83	10.56	9.39	7.66
7143	11.82	10.57	9.41	7.55
7436	11.84	10.57	9.44	7.67
7509	11.78	10.50	9.37	7.61
7749	11.83	10.53	9.37	7.63
7841	11.86	10.60	9.43	7.63
8132	11.78	10.52	9.36	7.67
8173	11.82	10.44	9.30	7.55
8573	11.78	10.49	9.33	7.61
8630	11.78	10.49	9.35	7.55
8875	11.77	10.51	9.38	7.61
8902	11.81	10.54	9.38	7.63
8906	11.77	10.52	9.40	7.63
8908	11.83	10.54	9.37	7.61
9258	11.83	10.55	9.39	7.62
9614	11.79	10.47	9.32	7.60
9615	11.78	10.48	9.30	7.59
9970	11.98	10.66	9.54	7.68
9971	11.93	10.69	9.57	7.75
10058	11.86	10.62	9.52	7.74
10117	11.86	10.57	9.48	7.72
10304	11.78	10.47	9.32	7.65
10410	11.79	10.50	9.36	7.55
10413	11.84	10.53	9.38	7.69
10655	11.89	10.67	9.51	7.70
10738	11.91	10.68	9.55	7.77
11115	11.85	10.68	9.64	7.95

Table 7. Fairall 9

MJD	<i>J</i>	<i>H</i>	<i>K</i>	<i>L</i>
3061	11.81	11.05	10.20	8.58
3510	11.80	10.64	09.73	8.40
3681	11.79	10.75	09.80	8.43
3683	11.85	10.75	09.84	8.44
4204	11.72	10.62	09.60	8.26
4469	11.89	10.69	09.64	8.37
5341	12.16	10.97	09.91	8.48
5619	12.35	11.25	10.18	8.52
5889	12.41	11.48	10.56	8.87
5890	12.46	11.45	10.52	
6047	12.46	11.63	10.75	
6287	12.36	11.50	10.68	9.16
6312	12.31	11.49	10.70	9.23
6313	12.38	11.50	10.68	9.17
6314	12.32	11.48	10.69	9.19
6476	12.38	11.42	10.54	8.98
6608	12.20	11.32	10.49	9.01
6662	12.24	11.28	10.42	8.94
6690	12.17	11.22	10.38	8.95
6767	12.09	11.20	10.32	8.93
6777	12.18	11.16	10.33	8.85
6850	12.14	11.17	10.35	8.85
6984	12.07	11.12	10.24	8.79
6985	12.07	11.11	10.21	8.99
7141	12.08	11.08	10.18	8.64
7143	12.08	11.08	10.16	8.76
7435	12.09	11.05	10.12	8.74
7436	12.03	11.05	10.12	8.73
7438	12.07	11.06	10.12	8.74
7509	12.12	11.03	10.11	8.85
7512	12.13	11.11	10.14	8.74
7580	12.15	11.07	10.16	8.65
7748	12.10	11.09	10.16	8.74
7749	12.11	11.10	10.18	8.73
7839	12.19	11.13	10.18	8.74
7842	12.18	11.14	10.19	8.75
7875	12.15	11.14	10.19	8.85
7876	12.13	11.13	10.19	8.73
7964	12.24	11.17	10.23	
8042	12.23	11.18	10.26	8.74
8170	12.06	11.04	10.15	8.75
8172	12.04	11.03	10.15	8.72
8173	12.05	11.05	10.14	8.72
8224	12.07	11.03	10.10	8.73
8529	12.04	11.06	10.11	8.72
8573	12.13	11.04	10.10	8.67
8576	12.12	11.04	10.10	8.57
8629	12.08	11.03	10.10	8.75
8633	12.09	11.03	10.13	8.66
8875	12.29	11.24	10.28	8.76
8877	12.26	11.21	10.27	8.75
8902	12.27	11.21	10.32	8.73
8905	12.33	11.28	10.30	8.85
8908	12.32	11.26	10.31	8.81
8995	12.28	11.26	10.37	8.84
9255	12.37	11.44	10.55	8.97
9609	12.28	11.33	10.47	9.00
9614	12.30	11.31	10.49	9.02
9889	11.90	11.01	10.15	8.84
9966	11.98	10.95	10.07	8.82
9972	11.97	10.95	10.08	8.80
10053	11.99	10.95	10.04	8.68
10113	11.99	10.95	10.04	8.63
10302	12.04	11.00	10.06	8.64
10410	12.08	11.04	10.08	8.62
10614	12.11	11.03	10.07	8.64
10655	12.24	11.17	10.19	8.77
10720	12.25	11.17	10.00	RAS, MNRAS 000, 000–000
10742	12.21	11.21	10.25	8.72
11118	12.37	11.49	10.65	9.09

Table 8. NGC 526a

MJD	<i>J</i>	<i>H</i>	<i>K</i>	<i>L</i>	<i>L</i> _{err}
4466	12.32	11.18	10.22		
			10.32	8.58	.10
4482					
4919	12.49	11.59	10.92		
5889	12.54	11.71	11.09	9.95	.15
5890	12.48	11.64	11.06		
6287	12.50	11.66	11.16	0.11	.20
6478	12.44	11.55	10.95		
6608	12.36	11.52	10.85	9.59	.11
6664	12.36	11.47	10.71	9.44	.07
6692	12.36	11.38	10.67	9.32	.07
6767	12.36	11.50	10.71	9.46	.09
6776	12.36	11.44	10.73	9.43	.15
6985	12.37	11.39	10.60	9.23	.05
7142	12.42	11.42	10.60	9.25	.08
7341	12.46	11.42	10.65	9.29	.08
7435	12.45	11.49	10.79	9.42	.04
7436	12.45	11.56	10.79	9.46	.07
7438	12.45	11.52	10.77	9.62	.09
7509	12.46	11.54	10.89	9.32	.12
7584		11.58	10.89	9.60	.18
7748	12.46	11.56	10.89	9.53	.06
7749	12.46	11.56	10.89	9.53	.06
7839	12.51	11.51	10.85	9.51	.09
7841	12.46	11.51	10.83	9.63	.03
7843	12.49	11.53	10.83	9.65	.10
7875	12.48	11.52	10.80	9.58	.08
7876	12.45	11.49	10.79	9.58	.10
8132	12.45	11.52	10.85	9.61	.05
8172	12.37	11.41	10.68	9.43	.06
8226	12.45	11.45	10.68	9.53	.05
8529	12.49	11.57	10.95	9.84	.10
8573	12.50	11.59	10.96	9.75	.10
8576	12.50	11.52	10.89	9.80	.13
8630	12.44	11.54	10.89	9.68	.10
8833	12.43	11.53	10.89	9.55	.08
8875	12.31	11.29	10.59	9.45	.03
8877	12.25	11.32	10.56	9.34	.05
8902	12.38	11.33	10.52	9.18	.06
8905	12.33	11.33	10.50	9.24	.05
8906	12.37	11.29	10.57	9.31	.05
8908	12.30	11.30	10.49	9.29	.07
9255	12.36	11.40	10.62	9.26	.05
9609	12.21	11.10	10.24	8.91	.03
9614	12.18	11.11	10.22	9.02	.04
9966	12.24	11.09	10.15	8.67	.05
9971	12.20	11.09	10.15	8.85	.07
10053	12.28	11.18	10.26	8.81	.04
10116	12.31	11.20	10.26	8.74	.06
10302	12.34	11.25	10.36	8.91	.05
10410	12.29	11.31	10.48	9.10	.06
10655	12.41	11.52	10.85	9.47	.08
10721	12.39	11.38	10.67	9.23	.09
10738	12.35	11.38	10.65	9.18	.09
11114	12.40	11.44	10.65	9.24	.02

Table 9. NGC985

MJD	<i>J</i>	<i>H</i>	<i>K</i>	<i>L</i>	<i>L</i> _{err}
7839	12.70	11.80	11.19	10.23	.11
9972	12.65	11.78	11.13	10.07	.08
10057	12.60	11.72	11.07	9.87	.13
10118	12.53	11.65	11.05	9.95	.12
10721	12.39	11.46	10.71	9.55	.09
11117	12.60	11.63	10.94	9.81	.06
11601	12.62	11.73	11.02	9.71	.24

Table 10. ESO198-G24

MJD	<i>J</i>	<i>H</i>	<i>K</i>	<i>L</i>	<i>L</i> _{err}
7842	12.88	11.92	11.10	9.75	.11
8575	12.91	12.00	11.29	9.91	.14
8576	12.96	12.03	11.26	10.25	.15
8630	12.93	12.03	11.27	9.97	.12
8875	12.94	12.06	11.27	10.10	.06
8902	12.95	12.12	11.36	10.15	.14
8906	13.00	12.08	11.29	10.10	.08
8908	13.09	12.17	11.33	10.26	.10
9255	12.83	12.03	11.24	10.09	.17
9614	13.18	12.30	11.52	10.03	.11
9970	13.22	12.22	11.51	10.09	.12
10053	13.16	12.29	11.51	10.14	.16
10116	13.22	12.29	11.58	10.31	.19
10304	13.12	12.21	11.52	10.24	.10
10413	13.37	12.25	11.51	10.25	.12
10721	13.32	12.57	12.02	10.85	.21
10738	13.45	12.58	11.98		
11117	13.08	12.13	11.37	10.42	.10

Table 11. NGC1068

MJD	<i>J</i>	<i>H</i>	<i>K</i>	<i>L</i>
0900	0.0	8.05	7.40	5.42
3024	9.13	8.18	7.47	5.51
6047	9.06	8.08	7.09	4.97
6314	9.05	8.09	7.10	4.96
7437	9.03	8.03	7.01	4.90
7842	9.07	8.08	7.03	4.88
7877	9.07	8.06	7.01	4.82
8173	9.02	8.03	6.97	4.82
8529	9.00	8.00	6.92	4.77
8575	9.05	8.02	6.93	4.78
8634	9.08	8.02	6.94	4.75
8875	9.04	7.99	6.90	4.74
8902	9.06	8.02	6.91	4.73
9615	9.04	7.99	6.87	4.66
9889	0.0	0.0	6.89	4.72
9895	9.12	8.02	6.91	4.70
9966	9.06	7.99	6.89	4.69
9971	9.09	8.01	6.89	4.71
10057	9.06	8.03	6.91	4.70
10114	9.07	8.04	6.93	4.69
10302	9.03	8.00	6.92	4.72
10410	9.04	8.04	6.95	4.75
10655	9.06	8.04	6.97	4.78
10863	9.09	8.10	7.07	4.80
10868	9.08	8.08	7.02	4.84
11115	9.00	8.01	7.04	4.84
11599	9.10	8.07	7.05	4.82
11600	9.05	8.06	7.03	4.81

Table 12. NGC1566

MJD	<i>J</i>	<i>H</i>	<i>K</i>	<i>L</i>	<i>L</i> _{err}
1569	10.59	9.66	9.41		
3024			9.48		
3025	10.64	9.80	9.50	8.77	.28
3718	10.59	9.78	9.53		
3887			9.70		
4466	10.65	9.81	9.53		
5266		0.0	9.51		
5302	10.64	9.79	9.36	8.70	.07
5341	10.69	9.83	9.38		
5420	10.72	9.91	9.54		
5740	10.78	9.93	9.62		
6050	10.69	9.89	9.62	9.38	.11
6059	10.70	9.88	9.61	9.30	.03
6117	10.66	9.89	9.64	9.35	.13
6287	10.71	9.93	9.62	9.51	.08
6479	10.73	9.89	9.62		
6664	10.69	9.88	9.60	9.36	.10
6691	10.73	9.92	9.62	9.34	.08
6777	10.69	9.91	9.64	9.23	.08
6846	10.68	9.89	9.62	9.27	.10
7143	10.65	9.83	9.45	8.87	.04
7247	10.67	9.88	9.58	9.04	.12
7435	10.72	9.86	9.58	9.21	.08
7509	10.70	9.87	9.61	9.07	.09
7581	10.73	9.90	9.63	9.30	.05
7749	10.70	9.88	9.59	9.35	.04
7842	10.73	9.88	9.60	9.20	.05
7876	10.74	9.90	9.62	9.50	.07
8173	10.72	9.90	9.61	9.26	.05
8576	10.71	9.87	9.60	9.31	.06
8630	10.71	9.86	9.59	9.25	.07
8875	10.73	9.89	9.62	9.32	.03
8902	10.74	9.91	9.63	9.37	.06
8995	10.70	9.87	9.62	9.19	.09
9255	10.66	9.88	9.63	9.26	.09
9971	10.72	9.87	9.57	9.40	.08
0053	10.71	9.88	9.59	9.30	.05
0114	10.69	9.87	9.60	9.47	.11
0411	10.71	9.88	9.60	9.14	.05
0509	10.64	9.87	9.55	9.19	.10
0721	10.69	9.87	9.56	9.10	.07
0868	10.69	9.87	9.56	9.40	.08
1117	10.70	9.85	9.60	9.43	.06
1601	10.67	9.83	9.53	9.11	.07
1602	10.78	9.91	9.59	8.92	.09

Table 13. 3C120

MJD	<i>J</i>	<i>H</i>	<i>K</i>	<i>L</i>	<i>L</i> _{err}
6049	12.32	11.30	10.28	8.86	.06
7143	12.48	11.49	10.54	9.08	.07
7437	12.42	11.36	10.43	9.05	.05
7580	12.59	11.53	10.49	9.18	.09
7749	12.40	11.45	10.52	8.99	.04
7839	12.37	11.36	10.45	9.06	.06
7968	12.46	11.43	10.45	9.10	.09
8172	12.42	11.35	10.40	8.97	.03
8529	12.66	11.61	10.59	8.95	.04
8575	12.58	11.60	10.59	9.05	.05
8629	12.65	11.61	10.62	9.12	.06
8633	12.62	11.59	10.65	9.12	.05
8634	12.64	11.60	10.66	9.13	.05
8874	12.42	11.58	10.71	9.26	.04
8902	12.47	11.51	10.68	9.12	.05
8908	12.39	11.50	10.64	9.22	.05
9255	12.16	11.21	10.29	8.98	.05
9615	12.46	11.38	10.34	8.83	.04
9970	12.36	11.32	10.37	8.97	.05
10114	12.38	11.36	10.39	8.76	.01
10410	12.34	11.32	10.40	8.89	.06
10507	12.26	11.25	10.32	8.86	.04
10657	12.21	11.18	10.21	8.79	.04
10720	12.26	11.17	10.18	8.82	.05
10738	12.30	11.18	10.23	8.69	.06
10863	12.36	11.29	10.29	8.74	.08
10868	12.36	11.31	10.33	8.85	.07
11115	12.36	11.32	10.32	9.08	.05
11599	12.50	11.41	10.45		
11600	12.46	11.44	10.44	9.02	.10

Table 14. Akn120

MJD	<i>J</i>	<i>H</i>	<i>K</i>	<i>L</i>
6780	11.65	10.67	9.81	8.57
7143	11.76	10.71	9.83	8.49
7244	11.67	10.70	9.80	8.55
7437	11.80	10.76	9.90	8.49
7513	11.70	10.73	9.85	8.60
7580	11.68	10.72	9.85	8.56
7839	11.57	10.57	9.70	8.43
7875	11.56	10.54	9.67	8.43
7876	11.64	10.55	9.70	8.47
7967	11.59	10.53	9.67	8.34
8172	11.57	10.53	9.66	8.29
8529	11.92	10.86	9.94	8.59
8575	11.92	10.92	10.02	8.67
8576	11.94	10.94	10.03	8.61
8629	11.93	10.92	10.06	8.63
8633	11.89	10.94	10.07	8.62
8874	11.75	10.77	9.96	8.70
8902	11.77	10.80	9.97	8.69
8995	11.83	10.82	9.96	8.72
9255	11.81	10.87	10.03	8.74
9615	11.96	10.97	10.14	8.83
9966	11.88	10.89	10.08	8.84
10113	11.96	10.93	10.11	8.88
10410	11.85	10.86	10.09	8.90
10507	11.80	10.83	10.02	8.72
10657	11.82	10.83	10.03	8.78
10720	11.80	10.85	10.02	8.71
10738	11.80	10.81	10.00	8.65
10863	11.76	10.81	10.02	8.66
10868	11.75	10.79	9.97	8.76
11115	11.82	10.84	10.05	8.84
11599	11.84	10.96	10.18	8.93

Table 15. MCG-5-13-17

MJD	<i>J</i>	<i>H</i>	<i>K</i>	<i>L</i>	<i>L</i> _{err}
6923	11.67	10.96	10.61	9.89	.05
7144	11.74	10.96	10.51	9.78	.17
7246	11.69	10.97	10.54	9.87	.10
7437	11.70	10.92	10.57	9.89	.08
7580	11.81	10.98	10.59	9.63	.05
7581	11.79	10.95	10.57	9.83	.08
7634	11.76	11.00	10.60	10.11	.08
7842	11.77	10.99	10.63	10.02	.10
7876	11.77	10.97	10.61	10.00	.10
7964	11.80	11.04	10.70	9.95	.16
8173	11.80	11.02	10.73	10.03	.11
8576	11.76	10.96	10.61	10.00	.10
8629	11.78	11.02	10.70	10.09	.14
8877	11.78	11.02	10.65	10.05	.12
8902	11.79	11.04	10.72	10.25	.10
8908	11.79	11.03	10.72	10.07	.12
9615	11.71	10.95	10.56	9.90	.11
10053	11.70	10.92	10.50	9.65	.08
10113	11.75	10.97	10.60	9.84	.05
10115	11.73	10.96	10.62	9.84	.15
10411	11.70	10.93	10.53	9.77	.11
10509	11.82	11.00	10.69	10.04	.2
10863	11.80	10.99	10.63	9.84	.17
11115	11.72	10.93	10.56	9.78	.09
11597	11.74	10.92	10.55	9.66	.15

Table 16. Pictor A

MJD	<i>J</i>	<i>H</i>	<i>K</i>	<i>L</i>
3887	14.04	12.98	11.92	
5743	14.07	12.94	11.89	
6050	13.95	12.99	12.05	
6776		12.93	11.97	
7144	14.04	12.95	11.81	
7247	13.92	12.88	11.88	
7584	14.12	13.17	12.13	
7842	13.94	12.97	12.05	
7877	13.96	12.98	12.06	
8579	14.21	13.05	12.14	
8630	13.88	12.99	12.05	
9971		12.86	11.89	
10115	14.01	12.88	12.07	
10509	13.85	12.96	12.01	
10600	14.18	13.06	12.09	
10721	13.79	12.93	11.96	
10866	13.87	12.81	11.90	10.34

Table 17. NGC2110

MJD	<i>J</i>	<i>H</i>	<i>K</i>	<i>L</i>
4320	10.83	9.86	9.44	
5266	10.79	9.88	9.50	
5343	10.84	9.90	9.48	8.68
7347	10.83	9.81	9.44	8.75
7580	10.82	9.86	9.44	8.76
7839	10.84	9.86	9.47	8.78
7876	10.84	9.87	9.45	8.74
7967	10.84	9.90	9.47	8.74
8172	10.82	9.86	9.45	8.80
8874	10.83	9.85	9.48	8.80
9972	10.82	9.85	9.43	8.64
10113	10.81	9.81	9.40	8.62
10507	10.83	9.86	9.44	8.74
11600	10.88	9.88	9.47	8.61
11602	10.79	9.83	9.44	8.52

Table 18. H0557-383

MJD	<i>J</i>	<i>H</i>	<i>K</i>	<i>L</i>
4974	12.23	11.22	10.05	8.28
5042	12.28	11.16	10.05	8.13
6050	12.47	11.33	10.18	8.32
6118	12.43	11.33	10.18	8.40
6780	12.27	11.16	9.99	8.27
6925	12.25	11.12	9.99	8.26
7243	12.37	11.24	10.09	8.24
7347	12.34	11.15	10.05	8.27
7579	12.41	11.21	10.08	8.31
7580	12.41	11.21	10.09	8.22
7634	12.37	11.15	10.06	8.24
7839	12.39	11.21	10.06	8.18
7876	12.43	11.26	10.10	8.30
7967	12.49	11.30	10.18	8.24
8173	12.53	11.35	10.23	8.35
8576	12.39	11.23	10.13	8.38
8629	12.35	11.17	10.11	8.31
8633	12.29	11.17	10.11	8.37
8634	12.30	11.18	10.09	8.28
8734	12.29	11.10	10.04	8.27
8875	12.32	11.12	10.00	8.25
8902	12.27	11.13	9.98	8.26
9255	12.41	11.28	10.11	8.30
9615	12.48	11.36	10.23	8.37
9971	12.33	11.16	10.05	8.44
10053	12.21	11.11	10.01	8.25
10113	12.25	11.05	9.95	8.30
10116	12.21	11.05	9.96	8.30
10411	12.20	11.06	9.93	8.16
10509	12.18	11.05	9.93	8.10
10742	12.27	11.11	10.01	8.27
11115	12.24	11.03	9.86	8.14
11597	12.41	11.22	10.09	8.25

Table 19. Fairall 265

MJD	<i>J</i>	<i>H</i>	<i>K</i>	<i>L</i>	<i>L</i> _{err}
5341	12.71	11.84	11.14		
6923	12.71	11.81	11.15	9.89	.17
7243	12.70	11.83	11.12	10.00	.10
7581	12.71	11.83	11.16	10.03	.07
7634	12.79	11.88	11.18		
7967	12.73	11.88	11.17	10.34	.16
8629	12.76	11.84	11.21	10.21	.14
8734	12.68	11.78	11.12	10.22	.12
10114	12.79	11.84	11.17	9.97	.16
10116	12.74	11.84	11.17	10.16	.18
10511	12.86	11.94	11.34	10.15	.20
10868	12.75	11.86	11.23	10.15	.13

Table 20. IRAS09149-6206

MJD	<i>J</i>	<i>H</i>	<i>K</i>	<i>L</i>
10114	11.71	10.61	9.46	7.90
10116	11.70	10.64	9.51	7.90
10213	11.68	10.60	9.50	7.93
10510	11.58	10.52	9.42	7.88
10867	11.75	10.37	9.25	7.72
10950	11.51	10.42	9.34	7.83
11597	11.74	10.57	9.39	7.90

Table 21. NGC2992

MJD	<i>J</i>	<i>H</i>	<i>K</i>	<i>L</i>	<i>L</i> _{err}
3596	11.02	10.06	9.40	8.30	.15
3681	11.15	10.17	9.50	8.38	.05
4318	11.16	10.16	9.63		
4920	11.20	10.29	9.80		
5082	11.07	10.15	9.60	8.42	.28
5340	11.20	10.23	9.58	8.69	.05
5740	11.18	10.16	9.63	8.60	.07
5845	11.23	10.24	9.76	8.78	.06
6117	11.19	10.21	9.68	8.55	.05
6194	11.10	10.09	9.53	8.68	.03
6476	11.18	10.20	9.69	8.84	.07
6478	11.17	10.19	9.68	8.77	.10
6581	11.16	10.19	9.69	8.94	.08
6610	11.21	10.20	9.69	8.99	.07
6846	11.20	10.24	9.78		
6850	11.19	10.27	9.81	9.14	.08
6923	11.15	10.19	9.73	9.03	.04
6989	11.18	10.21	9.77		
7163	11.23	10.35	9.43		
7212	10.92	9.95	9.27		
7243	11.00	09.93	9.21	8.16	.05
7247	10.99	09.93	9.23	8.21	.04
7248	11.00	09.94	9.25	8.22	.05
7342	11.17	10.13	9.48	8.29	.06
7343	11.17	10.14	9.50	8.41	.03
7509	11.12	10.09	9.45	8.41	.05
7580	11.21	10.17	9.58	8.53	.04
7581	11.18	10.13	9.58	8.57	.02
7629	11.13	10.13	9.55	8.51	.07
7839	11.16	10.18	9.67		
7964	11.18	10.17	9.63	8.64	.04
8042	11.19	10.22	9.72	8.80	.02
8576	11.22	10.21	9.74	8.99	.06
8629	11.23	10.22	9.74	8.90	.05
8633	11.20	10.20	9.74	8.86	.05
8674	11.30	10.32	9.86	9.01	.08
8731	11.21	10.19	9.76	9.08	.06
8733	11.24	10.23	9.81		
8734	11.19	10.21	9.78	9.14	.07
8995	11.19	10.20	9.76	8.94	.08
9890	11.24	10.24	9.80	9.34	.05
10053	11.23	10.19	9.73	9.22	.07
10113	11.20	10.21	9.75	9.11	.07
10213	11.23	10.21	9.81	9.22	.10
10411	11.21	10.22	9.75	9.14	.08
10507	11.24	10.23	9.78	9.26	.05
10509	11.21	10.22	9.76	9.13	.08
10615	11.24	10.21	9.79	9.09	.06
10863	11.15	10.23	9.79	9.21	.09
10948	11.18	10.16	9.75	9.07	.03
11599	11.19	10.19	9.65	8.87	.11

Table 22. MCG-5-23-16

MJD	<i>J</i>	<i>H</i>	<i>K</i>	<i>L</i>	<i>L</i> _{err}
3887	11.48	10.52	9.86	8.40	0.12
4001	11.40	10.48	9.85	8.44	0.12
5046	11.29	10.45	9.88		
6612	11.33	10.43	9.84	8.63	0.05
6886	11.39	10.53	10.03		
6923	11.34	10.50	9.95	8.62	0.04
6985	11.45	10.56	10.05	8.89	0.05
7246	11.32	10.41	9.87	8.65	0.05
7343	11.45	10.49	9.93	8.88	0.07
7581	11.42	10.58	10.13	9.03	0.03
7634	11.44	10.55	10.11	9.06	0.04
7876	11.40	10.52	10.05	9.03	0.08
7968	11.41	10.55	10.10	9.09	0.06
8629	11.39	10.51	10.01	8.84	0.06
8634	11.40	10.51	10.02	8.88	0.04
8671	11.39	10.52	10.01	9.04	0.07
8731	11.38	10.54	10.09		
8733	11.39	10.51	10.08	9.11	0.05
8734	11.39	10.50	10.08	8.95	0.06
10113	11.33	10.37	9.76	8.60	0.04
10213	11.32	10.40	9.82	8.65	0.03
10509	11.35	10.44	9.88	8.65	0.06
10866	11.35	10.40	9.81	8.45	0.04
10949	11.36	10.42	9.82	8.56	0.03
11597	11.35	10.46	9.90	8.84	0.08

Table 23. NGC3783

MJD	<i>J</i>	<i>H</i>	<i>K</i>	<i>L</i>
2225			9.55	
2822			9.71	8.69
3322	11.41	10.54	9.60	
3511			9.82	
3602	11.54	10.67	10.09	
3680			10.26	
3888			10.00	
4001	11.70	10.89	10.14	8.49
4266	11.38	10.45	9.71	
5081	11.17	10.21	9.40	8.05
5382	11.44	10.48	9.66	
5387	11.41	10.43	9.60	
5416	11.28	10.39	9.57	8.18
5687	11.39	10.48	9.69	
5740	11.45	10.57	9.80	8.41
5846	11.35	10.48	9.77	8.49
5886	11.36	10.45	9.75	8.52
5887	11.36	10.46	9.75	8.48
5889	11.32	10.43	9.72	8.34
6117	11.34	10.47	9.72	8.54
6122	11.33	10.49	9.78	8.46
6194	11.25	10.34	9.60	8.35
6195	11.33	10.34	9.60	8.32
6198	11.30	10.39	9.64	8.45
6199	11.28	10.36	9.60	8.34
6476	11.18	10.23	9.41	8.09
6477	11.21	10.24	9.41	8.06
6479	11.20	10.24	9.41	8.00
6580	11.25	10.28	9.47	8.23
6582	11.26	10.30	9.51	8.07
6607	11.31	10.34	9.52	8.18
6844	11.33	10.37	9.61	8.33
6845	11.30	10.36	9.58	8.33
6846	11.30	10.36	9.58	8.26
6848	11.29	10.37	9.58	8.27
6850	11.26	10.35	9.57	8.21
6886	11.25	10.35	9.57	8.27
6923	11.30	10.32	9.53	8.25
6984	11.39	10.45	9.61	8.26
6988	11.37	10.41	9.64	8.23
7243	11.33	10.43	9.67	8.29
7246	11.32	10.42	9.65	8.26
7247	11.32	10.42	9.66	8.31
7248	11.34	10.44	9.69	8.34
7342	11.42	10.56	9.87	8.49
7579	11.27	10.42	9.76	8.54
7580	11.27	10.44	9.78	8.60
7581	11.31	10.45	9.77	8.53
7584	11.26	10.43	9.73	8.45
7585	11.29	10.42	9.75	8.58
7628	11.16	10.28	9.55	8.30
7629	11.14	10.27	9.52	8.26
7634	11.14	10.27	9.54	8.27
7676	11.17	10.23	9.44	8.22
7748	11.21	10.28	9.49	8.18
7842	11.27	10.35	9.55	8.25
7876	11.28	10.35	9.56	8.22
7967	11.23	10.32	9.55	8.24
7968	11.23	10.30	9.53	8.23
8042	11.25	10.34	9.58	8.18
8227	11.10	10.17	9.36	7.99
8576	11.33	10.43	9.71	8.32
8593	11.41	10.52	9.76	8.37
8629	11.33	10.44	9.70	8.40
8630	11.37	10.44	9.71	8.35
8632	11.33	10.44	9.70	8.32
8633	11.35	10.43	9.70	8.34

Table 24. NGC3783 (contd.)

MJD	<i>J</i>	<i>H</i>	<i>K</i>	<i>L</i>
8634	11.34	10.45	9.71	8.37
8671	11.35	10.46	9.69	8.34
8674	11.32	10.42	9.67	8.29
8675	11.32	10.41	9.65	8.23
8700	11.40	10.45	9.70	8.39
8727	11.33	10.43	9.69	8.34
8731	11.34	10.45	9.72	8.31
8733	11.35	10.43	9.69	8.38
8734	11.33	10.45	9.70	8.39
8765	11.24	10.44	9.72	8.30
8768	11.28	10.47	9.72	8.36
8783	11.17	10.39	9.65	8.31
8786	11.09	10.27	9.62	8.32
8789	11.16	10.34	9.60	8.32
8790	11.07	10.27	9.58	8.24
8792	11.16	10.35	9.63	8.27
8804	11.13	10.29	9.59	8.22
8834	11.20	10.35	9.60	8.26
8993	11.22	10.21	9.36	8.00
9890	11.58	10.68	9.98	8.57
10113	11.48	10.53	9.82	8.45
10117	11.41	10.58	9.86	8.54
10214	11.46	10.59	9.93	8.58
10304	11.39	10.49	9.80	8.47
10411	11.33	10.44	9.75	8.53
10509	11.32	10.34	9.58	8.25
10615	11.35	10.36	9.55	8.16
10655	11.42	10.45	9.66	8.26
10657	11.42	10.45	9.64	8.19
10863	11.43	10.57	9.90	8.42
10948	11.40	10.48	9.79	8.38
11597	11.38	10.45	9.71	8.51
11600	11.31	10.46	9.94	8.46

Table 25. H1143-182

MJD	<i>J</i>	<i>H</i>	<i>K</i>	<i>L</i>	<i>L</i> _{err}
6611	12.84	12.00	11.33	10.33	.10
6582	12.90	12.00	11.36		
			11.35	10.43	.19
7246	12.96	12.06	11.36		
7581	12.91	12.10	11.41	10.36	.07
7634	12.94	12.04	11.35	10.63	.00
7967	13.00	12.15	11.42	10.14	.11
7968	12.99	12.15	11.40	10.23	.12
8042	12.87	12.12	11.38	10.27	.09
8633	12.73	11.90	11.13	10.01	.11
10114	13.43	12.47	11.77	10.44	.23
10214	13.40	12.55	11.79		
10510	13.13	12.34	11.64	10.72	.17
10615	13.32	12.39	11.63		
11599	13.10	12.19	11.54	10.00	.16

Table 26. I Zw 96

MJD	<i>J</i>	<i>H</i>	<i>K</i>
5083	13.18	12.39	11.91
5741	13.16	12.48	11.92
5846	13.14	12.34	11.88
5887	13.14	12.36	11.96
6120	13.16	12.42	11.95
6477	13.06	12.26	11.80
6578	13.00	12.25	11.81
6610	13.06	12.23	11.81
6923	13.04	12.22	11.77
7246	13.00	12.25	11.78
7634	13.09	12.20	11.81
10116	13.07	12.24	11.81
10510	13.12	12.25	11.85

Table 27. NGC4593

MJD	<i>J</i>	<i>H</i>	<i>K</i>	<i>L</i>
5081	11.08	10.28	09.80	
5419	11.20	10.36	09.87	08.90
6116	11.14	10.24	09.69	08.69
6117	11.15	10.27	09.71	08.88
6120	11.12	10.26	09.75	08.75
6122	11.15	10.28	09.76	08.81
6111	11.12	10.22	09.63	08.71
6112	11.11	10.23	09.67	08.61
6114	11.14	10.26	09.70	08.78
6194	11.22	10.43	09.92	08.99
6195	11.19	10.33	09.78	08.90
6199	11.22	10.37	09.89	09.06
6477	11.11	10.26	09.73	08.88
6478	11.10	10.23	09.72	08.84
6479	11.12	10.25	09.74	08.88
6582	11.05	10.12	09.54	08.54
6609	11.06	10.16	09.56	08.73
6845	11.08	10.18	09.68	08.51
6923	11.11	10.24	09.68	08.61
6985	11.07	10.20	09.67	08.60
6988	11.08	10.24	09.69	08.71
7246	11.05	10.16	09.59	08.52
7584	11.21	10.33	09.87	08.95
7634	11.20	10.32	09.89	08.99
7967	11.21	10.35	09.93	09.03
7968	11.20	10.35	09.92	09.25
8042	11.22	10.33	09.91	09.14
8630	11.09	10.20	09.65	08.69
8634	11.10	10.18	09.64	08.78
8671	11.14	10.23	09.70	08.82
8674	11.18	10.22	09.70	08.79
8727	11.13	10.23	9.77	8.82
8731	11.10	10.22	9.72	8.83
8733	11.16	10.23	9.73	8.78
8734	11.10	10.22	9.73	8.86
9890	11.12	10.20	9.68	8.77
10114	11.11	10.17	9.62	8.57
10509	11.10	10.13	9.53	8.38
10615	11.05	10.15	9.65	8.58
10657	11.09	10.18	9.64	8.53
10948	11.10	10.19	9.63	8.59

Table 28. NGC4748

MJD	<i>J</i>	<i>H</i>	<i>K</i>	<i>L</i>	<i>L</i> _{err}
6194	12.05	11.25	10.76	10.15	0.21
6197	12.05	11.26	10.76	10.05	0.09
6923	12.16	11.36	10.98	10.37	0.12
6984	12.16	11.38	10.98	10.46	0.21
7246	12.12	11.35	10.91		
7579	12.17	11.36	10.98		
7580	12.17	11.39	11.02	10.54	0.14
7634	12.15	11.31	10.94	10.51	0.11
7967	12.20	11.35	10.99	11.44	0.11
8042	12.20	11.36	11.02	10.43	0.10
8674	12.21	11.39	11.03		
8734	12.19	11.41	11.04	10.79	0.30
10115	12.21	11.37	11.02	10.60	0.26
10510	12.17	11.35	10.97	10.58	0.15

Table 29. ESO323-G77

MJD	<i>J</i>	<i>H</i>	<i>K</i>	<i>L</i>	<i>L</i> _{err}
6886	10.80	9.64	8.75	7.50	
6923	10.79	9.63	8.75	7.49	
6984	10.80	9.61	8.70	7.45	
6989	10.88	9.67	8.79	7.57	
7245	10.80	9.67	8.76	7.57	
7246	10.83	9.70	8.80	7.56	
7342	10.88	9.76	8.85	7.62	
7580	10.88	9.74	8.86	7.56	
7634	10.89	9.72	8.84	7.56	
7967	10.94	9.83	8.96	7.75	
8042	10.96	9.84	8.96	7.75	
8629	11.00	9.88	9.03	7.75	
8633	11.00	9.89	9.04	7.73	
8674	10.99	9.89	9.04	7.72	
8675	10.99	9.89	9.03	7.77	
8731	10.98	9.86	9.01	7.78	
8733	10.93	9.81	8.94	7.71	
8734	10.99	9.85	8.98	7.78	
9889	11.05	9.96	9.14	7.94	
10114	11.02	9.92	9.10	7.87	
10304	11.07	9.98	9.16	8.00	
10509	11.04	9.94	9.13	7.94	
10614	11.08	9.97	9.14	7.96	
10656	11.07	9.98	9.17	7.95	
10863	11.09	10.02	9.19	7.83	
10948	11.10	10.03	9.18	8.03	
11599	11.00	9.96	9.18	7.93	

Table 30. MCG-6-30-15

MJD	<i>J</i>	<i>H</i>	<i>K</i>	<i>L</i>	<i>L</i> _{err}
3887	11.60	10.65	9.87	8.52	.10
4318	11.42	10.50	9.75		
4720	11.36	10.47	9.84		
5849	11.50	10.62	9.97	8.64	.05
5887	11.51	10.66	10.00	8.76	.05
5889	11.53	10.66	9.98	8.78	.07
6117	11.40	10.51	9.83	8.59	.05
6194	11.42	10.55	9.87	8.71	.04
6195	11.42	10.51	9.88	8.56	.05
6476	11.46	10.53	9.82	8.50	.06
6478	11.50	10.54	9.85	8.59	.08
6582	11.37	10.52	9.90	8.60	.03
6610	11.43	10.55	9.91	8.59	.06
6845	11.51	10.61	9.95	8.72	.05
6848	11.48	10.60	9.97	8.73	.06
6923	11.45	10.60	9.97	8.74	.05
6984	11.40	10.53	9.92	8.67	.05

MJD	<i>J</i>	<i>H</i>	<i>K</i>	<i>L</i>	<i>L</i> _{err}
7243	11.43	10.50	9.84	8.60	.03
7581	11.48	10.59	9.88	8.60	.04
7967	11.44	10.56	9.87	8.60	.04
8042	11.55	10.60	9.96	8.70	.04
8731	11.51	10.55	9.91	8.73	.04
10117	11.52	10.53	9.84	8.70	.03
10510	11.48	10.50	9.85	8.65	.04
10948	11.39	10.55	9.87	8.57	.02

Table 31. IC4329a

MJD	<i>J</i>	<i>H</i>	<i>K</i>	<i>L</i>	<i>L</i> _{err}
3325	11.14	10.22	9.38	7.93	
3602	11.12	10.27	9.38	7.80	
3682	11.16	10.19	9.32	7.90	
4320	11.00	10.02	9.12		
4323		9.29	7.57		
4720	11.02	10.06	9.16		
5849	10.94	9.97	9.09	7.64	
5887	10.93	9.94	9.04	7.59	
5889	10.94	9.95	9.05	7.65	
6194	11.06	10.00	9.10		
6195	10.96	9.99	9.12	7.61	
6216	10.95	10.00	9.10	7.55	
6607	11.04	10.03	9.13	7.56	
6845	11.02	10.03	9.14	7.72	
6849	11.07	10.03	9.15	7.66	
6923	11.09	10.11	9.23	7.77	
6925	11.07	10.10	9.22	7.68	
6984	11.11	10.14	9.26	7.80	
7243	11.06	10.13	9.29	7.80	
7342	10.99	10.06	9.24	7.77	
7581	11.05	10.03	9.14	7.68	
7584	11.07	10.04	9.15	7.67	
7634	11.05	10.02	9.15	7.73	
7967	10.94	9.92	9.04	7.54	
8042	10.94	9.95	9.05	7.62	
8630	10.88	9.84	8.92	7.39	
8632	10.91	9.86	8.93	7.48	
8633	10.90	9.85	8.93	7.39	
8671	10.87	9.85	8.93	7.43	
8731	10.87	9.84	8.92	7.47	
8734	10.89	9.83	8.93	7.42	
9889	10.95	10.02	9.14	7.63	
10114	11.01	10.04	9.21	7.60	
10304	10.91	9.92	9.05	7.60	
10509	11.07	10.04	9.16	7.59	
10614	11.03	10.04	9.12	7.61	
10656	10.97	10.00	9.10	7.60	
10948	10.97	9.94	9.04	7.54	
11600	10.93	9.94	9.05	7.56	

Table 32. NGC5506

MJD	<i>J</i>	<i>H</i>	<i>K</i>	<i>L</i>	<i>L</i> _{err}
3523		10.33	9.08	7.37	
3525	11.69	10.30	9.06	7.35	
5104	11.51	9.99	8.68	7.13	
5846	11.67	10.23	8.97	7.26	
5886	11.64	10.19	8.96	7.33	
5890	11.62	10.21	8.96	7.32	
6116	11.42	9.89	8.62	7.05	
6117	11.43	9.92	8.66	7.08	
6122	11.45	9.92	8.68	7.06	
6107	11.34	9.81	8.56	7.05	
6110	11.39	9.87	8.62	7.17	
6112	11.40	9.87	8.64	7.10	
6198	11.47	9.99	8.76	7.17	
6477	11.41	9.87	8.62	7.08	
6582	11.49	9.99	8.70	7.12	
6609	11.47	9.98	8.72	7.13	
6845	11.32	9.71	8.38	6.86	
6846	11.33	9.72	8.40	6.82	
6847	11.35	9.75	8.44	6.91	
6850	11.32	9.71	8.39	6.88	
6923	11.46	9.90	8.56	6.96	
6925	11.49	9.90	8.57	7.02	
6984	11.46	9.93	8.60	7.05	
6989	11.47	9.89	8.59	6.96	
7243	11.43	9.89	8.58	6.99	
7581	11.55	9.88	8.55	7.01	
7584	11.50	9.86	8.55	6.92	
7628	11.47	9.86	8.56	6.94	
7634	11.46	9.87	8.55	6.94	
7967	11.50	9.97	8.67	7.02	
8042	11.44	10.00	8.67	7.09	
8671	11.56	10.03	8.77	7.13	
8674	11.53	10.01	8.74	7.15	
8733	11.59	9.99	8.72	7.15	
8734	11.50	9.95	8.69	7.12	
9890	11.51	10.14	8.83	7.23	
9891	11.64	10.15	8.86	7.18	
10117	11.61	10.12	8.82	7.16	
10213	11.58	10.10	8.80	7.13	
10509	11.59	10.17	8.93	7.33	
10615	11.62	10.17	8.94	7.26	
10657	11.63	10.14	8.89	7.29	
10949	11.65	10.18	8.97	7.32	
11599	11.46	9.96	8.74	7.22	

Table 33. NGC5548

MJD	<i>J</i>	<i>H</i>	<i>K</i>	<i>L</i>	<i>L</i> _{err}
7243	11.62	10.81	10.10	8.91	
7246	11.62	10.83	10.10	8.83	
7241	11.61	10.79	10.08	8.67	
7248	11.59	10.78	10.08	8.74	
7342	11.66	10.80	10.06	8.65	
7581	11.67	10.81	10.06	8.79	
7584	11.69	10.76	10.02	8.89	
7628	11.59	10.71	9.99	8.65	
7634	11.63	10.71	9.98	8.84	
7748	11.67	10.71	9.94	8.56	
7967	11.81	10.88	10.13	8.77	
8042	11.79	10.96	10.29	9.00	

Table 34. IRAS15091-2107

MJD	<i>J</i>	<i>H</i>	<i>K</i>	<i>L</i>	<i>L</i> _{err}
6194	12.62	11.61	10.75	9.40	.07
6923	12.65	11.68	10.79	9.43	.06
6984	12.75	11.81	10.86	9.42	.06
7247	12.68	11.73	10.92	9.57	.08
7585	12.77	11.82	11.02		
7634	12.66	11.74	10.91	9.45	.08
8733	12.74	11.68	10.78	9.42	.09
9891	12.51	11.66	10.95	9.60	.07
10509	12.58	11.57	10.75		
10656	12.54	11.62	10.75	9.54	.07

Table 35. ESO103-G35

MJD	<i>J</i>	<i>H</i>	<i>K</i>	<i>L</i>	<i>L</i> _{err}
4320	12.37	11.50	11.07		
5844	12.22	11.43	11.03	9.73	.11
6197	12.25	11.46	11.04	9.68	.08
6608	12.25	11.47	11.09		
6691	12.33	11.43	11.05	9.55	.13
6923	12.25	11.43	11.03	9.70	.09
6984	12.33	11.50	11.10	9.73	.07
7243	12.26	11.40	11.05	9.75	.13
7343	12.27	11.49	11.05	9.77	.13
7433	12.30	11.44	11.06	9.78	.05
7749	12.24	11.44	11.05	9.72	.09
8042	12.25	11.43	11.02	9.73	.09
8132	12.23	11.41	11.05	9.74	.07
8167	12.24	11.43	11.06	9.66	.05
8173	0.0	0.0	11.06	9.55	.09
8528	12.25	11.45	11.07	9.88	.13
8731	12.28	11.45	11.06	9.63	.13
8733	12.31	11.44	11.08	9.73	.08
9615	12.26	11.42	11.04	9.64	.10
9889	12.21	11.42	11.02	9.75	.10
9966	12.27	11.44	11.02	9.76	.10
10212	12.27	11.42	11.05	9.76	.11
10304	12.26	11.40	11.02	9.80	.10
10615	12.30	11.42	11.03	9.79	.10
10656	12.23	11.38	11.01	9.78	.09
10948	12.27	11.43	11.05	9.63	.06

Table 36. Fairall 51

MJD	<i>J</i>	<i>H</i>	<i>K</i>	<i>L</i>	<i>L</i> _{err}
3029	12.01	10.88	9.92	8.45	.09
4320	12.10	11.00	10.07		
5595	12.02	11.00	10.20	8.70	.03
5887	11.99	11.01	10.12	8.79	.05
6923	12.04	11.09	10.29	8.95	.06
6984	12.07	11.13	10.29	9.07	.03
7243	12.00	11.08	10.26	8.97	.07
7342	11.99	11.01	10.17	8.85	.06
7343	11.98	10.99	10.22	8.81	.05
7433	11.98	10.97	10.11	8.78	.05
7749	11.94	10.90	10.04	8.68	.03
7842	12.09	11.10	10.25	8.83	.06
7967	11.88	10.81	9.96	8.63	.06
8042	11.91	10.87	9.98	8.60	.03
8132	11.95	10.88	10.01	8.65	.03
8167	11.93	10.88	9.98	8.67	.04
8528	11.95	10.92	10.06	8.72	.05
8731	12.02	10.95	10.04	8.75	.04
8733	11.97	10.92	10.03	8.71	.04
8734	11.97	10.91	10.01	8.69	.06
8875	12.00	10.99	10.14	8.84	.03
9889	12.14	11.04	10.17	8.80	.06
9966	12.17	11.14	10.26	8.75	.05
9972	12.15	11.12	10.28	8.89	.05
10213	12.06	10.99	10.16	8.80	.05
10304	11.94	10.86	9.99	8.77	.04
10614	11.94	10.90	10.06	8.74	.04
10656	11.96	10.90	10.04	8.76	.03
10948	12.01	10.93	10.01	8.66	.03

Table 37. ESO141-G55

MJD	<i>J</i>	<i>H</i>	<i>K</i>	<i>L</i>	<i>L</i> _{err}
4320	12.00	10.98	10.05		
5238	12.17	11.08	10.08		
5596	12.42	11.42	10.42	8.94	.04
5889	12.26	11.29	10.39	8.96	.05
6197	12.18	11.21	10.27	8.92	.02
6664	12.41	11.38	10.41	9.00	.06
6694	12.38	11.41	10.47	9.15	.12
6923	12.18	11.31	10.40	9.06	.07
6984	12.27	11.26	10.36	8.97	.04
7243	12.29	11.31	10.33	8.93	.08
7342	12.55	11.51	10.52	9.01	.07
7343	12.53	11.47	10.57	9.10	.07
7433	12.43	11.53	10.62	9.08	.03
7435	12.40	11.45	10.56	9.19	.06
7748	12.21	11.37	10.50	9.16	.05
7842	12.25	11.27	10.39	9.03	.06
7967	12.36	11.36	10.43	9.15	.07
8042	12.30	11.38	10.48	9.09	.04
8132	12.30	11.33	10.46	9.15	.04
8167	12.31	11.36	10.48	9.14	.05
8528	12.35	11.36	10.44	9.04	.07
8731	12.27	11.23	10.38	9.09	.06
8734	12.23	11.25	10.35	9.01	.07
8874	12.22	11.23	10.33	9.02	.03
9255	12.25	11.33	10.45	9.06	.06
9610	12.35	11.32	10.35	9.07	.04
9889	12.59	11.56	10.64	9.15	.07
9966	12.59	11.64	10.76	9.51	.08
9972	12.53	11.63	10.75	9.21	.05
10212	12.40	11.53	10.68	9.42	.12
10302	12.45	11.46	10.63	9.39	.06
10614	12.28	11.31	10.45	9.13	.03
10655	12.19	11.27	10.44	9.17	.07
10948	12.40	11.43	10.51	9.16	.03

Table 38. NGC6814

MJD	<i>J</i>	<i>H</i>	<i>K</i>	<i>L</i>	<i>L</i> _{err}
3024	11.53	10.47	10.14		
3683	11.53	10.71	10.32	9.80	.25
5585	11.29	10.44	10.02	9.45	.00
5888	11.37	10.47	10.06		
6191	11.40	10.53	10.20	9.76	.08
6287	11.44	10.58	10.25	9.73	.13
6329	11.41	10.58	10.29	10.00	.15
6984	11.41	10.58	10.31	10.01	.09
7749	11.39	10.53	10.22	9.82	.06
7968	11.40	10.54	10.20	9.85	.14
8042	11.42	10.53	10.19	9.80	.10
8132	11.45	10.54	10.20	9.89	.07
8167	11.42	10.52	10.23	9.61	.08
8172			10.21	9.80	.07
8733	11.48	10.59	10.31	9.94	.09
8876	11.43	10.55	10.29	9.98	.06
9614	11.44	10.57	10.30	9.96	.14
9889	11.39	10.52	10.19	9.91	.12
9966	11.35	10.40	10.00	9.52	.10
10059			10.15		
10213	11.41	10.54	10.28	10.27	.18
10302	11.41	10.55	10.31	10.10	.13
10614	11.40	10.52	10.25	9.89	.09
10655	11.34	10.45	10.07	9.64	.08
10742	11.41	10.54	10.16	9.61	.22
10949	11.39	10.51	10.14	9.62	.06

Table 39. MKN509

MJD	<i>J</i>	<i>H</i>	<i>K</i>	<i>L</i>
5235	11.98	11.07	10.20	
5236	11.96	11.06	10.19	
5237	11.97	11.05	10.17	
5238	12.01	11.08	10.19	
5239	11.96	11.08	10.18	
5240	11.97	11.09	10.20	
5595	11.80	10.87	09.98	8.69
6195	11.91	10.92	09.96	8.58
6197	11.94	10.93	09.96	
6287	11.97	11.01	10.04	8.59
6663	11.92	11.02	10.11	8.63
6694	11.92	11.01	10.12	8.76
6985	11.93	10.99	10.11	8.78
7342	11.93	11.08	10.18	8.90
7436	12.10	11.03	10.13	8.78
7634	11.98	11.01	10.09	
7749	12.01	11.02	10.13	8.77
7840	12.07	11.10	10.19	8.71
7841	12.05	11.10	10.18	8.68
8042	11.89	11.00	10.11	8.74
8132	11.80	10.92	10.05	8.72
8167	11.85	10.89	10.04	8.78
8172	11.81	10.88	10.02	8.65
8572	12.15	11.23	10.37	8.88
8574	12.13	11.25	10.38	8.90
8576	12.09	11.25	10.37	8.86
8733	12.07	11.14	10.32	8.90
8734	12.05	11.17	10.32	8.87
8875	11.89	11.00	10.19	8.85
8876	11.83	10.98	10.19	8.92
8905	11.85	10.95	10.11	
9609	12.03	11.10	10.19	8.81
9614	12.08	11.10	10.18	8.80
9889	12.01	11.01	10.10	8.80
9891	11.97	11.01	10.10	8.80
9966	11.93	11.01	10.12	8.70
10212	11.94	11.04	10.14	8.68
10394	11.96	10.99	10.12	8.80
10614	12.24	11.27	10.37	8.97
10655	12.16	11.23	10.37	8.95
10720	12.06	11.19	10.33	8.89
10749	12.09	11.22	10.33	
10948	12.01	11.09	10.25	8.81
11117	11.99	11.00	10.10	8.87

Table 40. H2107-097

MJD	<i>J</i>	<i>H</i>	<i>K</i>	<i>L</i>	<i>L</i> _{err}
6696	12.38	11.42	10.54	9.36	.09
7841	12.35	11.34	10.51	9.26	.08
9971	12.40	11.44	10.55	9.14	.07
10304	12.43	11.45	10.61	9.25	.07
10656	12.51	11.64	10.81	9.46	.06
10657	12.60	11.62	10.82		
10948	12.64	11.61	10.84	9.45	.03

Table 41. 1H2129-624

MJD	<i>J</i>	<i>H</i>	<i>K</i>	<i>L</i>	<i>L</i> _{err}
6691	13.34	12.31	11.43	9.95	.09
8875	13.02	11.94	11.09	9.84	.06
9615	13.51	12.60	11.81	10.26	.12
10304	13.15	12.28	11.60	10.54	.14
10658	13.28	12.33	11.48	10.28	.13
10949	13.33	12.47	11.70	10.32	.18

Table 42. NGC7213

MJD	<i>J</i>	<i>H</i>	<i>K</i>	<i>L</i>
3024	10.04	9.26	8.95	
4466	9.98	9.21	8.81	
5304	10.03	9.28	8.86	8.12
5305	10.05	9.29	8.85	8.15
5890	10.02	9.20	8.83	8.17
6197	10.06	9.24	8.87	8.20
6287	10.00	9.20	8.83	8.15
6582	10.02	9.20	8.80	8.11
6692	10.04	9.23	8.85	8.18
6780	10.07	9.23	8.84	8.18
6984	10.04	9.24	8.87	8.12
7342	10.05	9.25	8.85	8.10
7437	10.05	9.22	8.85	8.15
7749	10.03	9.21	8.82	8.06
7843	10.00	9.18	8.79	7.99
8173	10.06	9.18	8.79	7.99
8529	10.07	9.22	8.87	8.16
8575	10.07	9.25	8.88	8.17
8874	10.05	9.23	8.88	8.23
8905	10.08	9.25	8.92	8.27
9614	10.07	9.27	8.94	8.25
9890	10.09	9.27	8.96	8.45
9970	10.08	9.26	8.95	8.27
10213	10.07	9.24	8.95	8.32
10304	10.10	9.27	8.97	8.39
10658	10.06	9.26	8.93	8.38

Table 43. NGC7469

MJD	<i>J</i>	<i>H</i>	<i>K</i>	<i>L</i>
5279			9.28	8.21
5595	10.96	9.98	9.32	8.22
5887	10.91	9.94	9.22	8.10
5890	10.93	9.92	9.20	8.12
6197	10.97	9.98	9.26	8.13
6287	10.92	9.92	9.19	8.04
6663	11.00	10.01	9.33	8.18
6695	11.04	10.02	9.34	8.17
6778	10.99	10.05	9.36	8.26
6984	11.00	10.01	9.36	8.18
7342	11.00	10.05	9.43	8.18
7436	11.06	10.05	9.40	8.31
7753	11.12	10.22	9.72	8.85
7841	11.12	10.24	9.71	8.64
8132	11.00	10.01	9.35	8.28
8172	11.07	10.06	9.41	8.31
8529	10.95	9.94	9.21	8.04
8574	10.98	9.94	9.23	8.09
8874	10.95	9.95	9.27	8.08
8908	10.99	9.96	9.28	8.09
9614	11.05	10.02	9.35	8.20
9889	11.00	10.03	9.43	8.27
9966	10.98	10.00	9.30	8.14
10057	11.01	10.04	9.35	8.20
10212	10.95	9.98	9.28	8.19
10262	10.96	9.99	9.27	8.07
10302	11.00	10.01	9.36	8.18
10413	10.92	9.93	9.25	8.16
10614	10.93	9.92	9.22	8.06
10655	10.89	9.93	9.23	8.09
10721	10.81	9.83	9.11	7.97
10738	10.83	9.84	9.09	7.90
11114	10.91	9.86	9.09	7.97

Table 44. MCG-2-58-22

MJD	<i>J</i>	<i>H</i>	<i>K</i>	<i>L</i>	<i>L</i> _{err}
4484	12.45	11.45	10.54	9.10	.09
4466	12.34	11.43	10.52		
5887	12.08	11.16	10.32	9.08	.06
5890	12.15	11.18	10.32	9.15	.04
6197	12.11	11.12	10.20	8.99	.05
6287	12.10	11.12	10.17	9.06	.04
6664	12.20	11.24	10.25	8.99	.08
6692	12.14	11.16	10.22	8.95	.05
6778	12.34	11.24	10.29	8.81	.05
6984	12.49	11.47	10.48	9.03	.10
7142	12.62	11.64	10.72	9.22	.08
7341	12.59	11.70	10.83	9.42	.06
7342	12.72	11.73	10.91	9.35	.09
7435	12.65	11.74	10.85	9.45	.08
7346	12.63	11.73	10.87	9.43	.10
7509	12.57	11.70	10.87	9.30	.08
7748	12.76	11.84	10.99	9.63	.11
7841	12.73	11.90	11.07	9.68	.09
7843	12.80	11.85	11.09	9.76	.12
7875	12.79	11.90	11.13	0.02	.13
7876	12.78	11.88	11.12	9.45	.10
8042	12.68	11.80	11.07	9.68	.07
8132	12.64	11.72	10.93	9.61	.06
8172	12.66	11.73	10.96	9.60	.06
8173	12.66	11.76	10.94	9.63	.07
8224	12.65	11.76	10.94	9.52	.08
8529	12.49	11.57	10.69	9.33	.03
8574	12.50	11.52	10.70	9.41	.09
8576	12.52	11.54	10.69	9.55	.09
8874	12.54	11.56	10.66	9.36	.04
8876	12.58	11.54	10.68	9.37	.05
8902	12.76	11.60	10.66	9.33	.08
8906	12.63	11.60	10.74	9.48	.06
8908	12.63	11.62	10.73	9.41	.07
9258	12.88	11.90	11.12	9.51	.15
9609	12.82	11.95	11.32	10.05	.10
9615	12.95	11.95	11.26	9.97	.13
9889	12.66	11.84	11.13	9.87	.12
9966	12.78	11.88	11.17	9.89	.01
10053	12.84	11.91	11.18	9.58	.12
10214	12.86	11.88	11.23	10.20	.13
10302	12.84	11.89	11.22	10.09	.10
10410	12.88	11.92	11.28	9.98	.12
10614	12.82	11.89	11.24	10.25	.13
10655	12.79	11.87	11.26	10.16	.09
10720	12.76	11.84	11.15	9.96	.11
10741	12.88	11.81	11.15		
10948	12.83	11.92	11.19	9.94	.10
11115	12.81	11.93	11.34	10.25	.10

Table 45. NGC7603

MJD	<i>J</i>	<i>H</i>	<i>K</i>	<i>L</i>	<i>L</i> _{err}
3719	11.90	11.15	10.76		
5886	11.98	11.11	10.61		
6049	11.87	10.99	10.42		
6287	11.85	10.86	10.37	9.10	.05
6663	11.90	11.06	10.51		
6693	11.84	10.98	10.40	9.51	.20
6984	11.94	11.03	10.43	9.50	.08
7142	11.88	11.04	10.41	9.63	.22
7437	12.01	11.10	10.59	9.66	.12
7843	11.93	11.09	10.62	9.73	.13
8132	12.00	11.08	10.53	9.62	.04
8172	11.95	11.06	10.51	9.75	.06
8529	11.88	11.01	10.43	9.47	.07
8575	11.93	11.05	10.45	9.54	.10
8874	11.88	10.99	10.48	9.46	.04
9615	11.88	10.93	10.24	8.99	.04
9889	11.89	10.97	10.46	9.47	.09
9966	11.86	10.98	10.42	9.27	.08
10058	11.70	10.85	10.26	9.07	.07
10302	11.77	10.79	10.09	8.94	.05
10413	11.82	10.86	10.14	8.94	.05
10614	11.72	10.76	10.09	8.93	.05
10655	11.72	10.81	10.10	8.88	.05
10720	11.70	10.76	10.03	8.95	.07
10738	11.72	10.78	10.04	8.79	.10
11114	11.61	10.65	9.89	8.80	.05